Gas geochemistry of hydrothermal fluids of the S. Miguel and Terceira Islands, Azores

Stefano Caliro[a,*], Fátima Viveiros[b], Giovanni Chiodini[c] and Teresa Ferreira[b]

[a] Istituto Nazionale di Geofisica e Vulcanologia (INGV), Sezione di Napoli, Osservatorio Vesuviano, Via Diocleziano 328, 80124 Napoli, Italy

[b] Centro de Vulcanologia e Avaliação de Riscos Geológicos, Universidade dos Açores, Rua da Mãe de Deus, 9501-801 Ponta Delgada, Portugal

[c] Istituto Nazionale di Geofisica e Vulcanologia (INGV), Sezione di Bologna, Via Donato Creti 12, 40128 Bologna, Italy

***Corresponding author: Stefano Caliro**

Istituto Nazionale di Geofisica e Vulcanologia (INGV)

Sezione di Napoli

Osservatorio Vesuviano

Via Diocleziano 328

80124 Napoli, Italy.

E-mail: stefano.caliro@ingv.it

Tel: +39-081-6108425

Fax: +39-081-6108466

Abstract

We present here for the first time a complete dataset of the chemical and isotopic compositions of fumarolic fluids collected on the S. Miguel (Fogo and Furnas volcanoes) and Terceira (Pico Alto volcano) Islands. The data are analysed and discussed, to provide both a comprehensive picture of the thermodynamic conditions of the hydrothermal systems on these two islands, and to give new insight into the origins of these fluids, for a better understanding of the geodynamic context of the Azores archipelago. For S. Miguel Island, the gas equilibria in the H_2-CO_2-CO-CH_4-H_2O system suggest temperatures of the hydrothermal system reservoirs from 190 °C to 280 °C for the Fogo volcano fumaroles, which are 30 °C to 35 °C higher than those measured for geothermal wells. The equilibrium temperatures estimated for the Furnas volcano hydrothermal system are from 200 °C to 275 °C. Equilibrium vapor at a temperature of ~ 190 °C is inferred for the fumarolic fluids discharged on Terceira Island.

The He isotopic composition of ~9.6 *R/Ra* measured in the fumaroles of Terceira suggests that a plume-like source, presumably from the lower mantle, feeds this hydrothermal system. The relatively low $^3He/^4He$ ratios (from 5.21 to 5.35 *R/Ra)* and higher $CO_2/^3He$ ratios of S. Miguel fluids suggest an addition of ~ 45% of radiogenic He and ~30% of crustal CO_2 to a plume-like composition as at Terceira.

A mainly meteoric origin is inferred for the fumarolic water, whereas the unreactive gas species (He, Ar, N_2) arise from mixing processes between an atmospheric-like component and a magmatic component. On S. Miguel Island, the estimated magmatic fluid composition in terms of the ratios of $N_2/^{40}Ar$ (62 ±6) suggests a plume-like mantle source. Deep derived N_2 isotope compositions characterized by very negative $\delta^{15}N$ values ($\delta^{15}N \leq -14‰$) are inferred for the fluids of the Terceira Island. Also S. Miguel fluids are compatible with the same source with a possible involvement of crustal-derived Nitrogen. These values are more negative than the typical compositions of both the upper mantle and plume-like mantle, which thus supports the possible presence of a ^{15}N-depleted source, presumably from the lower mantle, in the region.

1. Introduction

Located in the triple junction domain of the Eurasian, North American and Nubian plates (Searle, 1980), the Azores Islands are the emerged peaks of various volcanic ridges that overlapped during the formation of the Azores Plateau (Fig. 1), an area of anomalous oceanic crust thickening (Luis et al., 1998). The source of the Azores volcanism has been attributed to the presence of a mantle plume (e.g., Schilling, 1975; Cannat et al., 1999; Gente et al., 2003; Madureira et al., 2005; 2014; Yang et al., 2006), although this remains under intense debate (Schilling et al., 1980; Bonatti, 1990; Mètrich et al., 2014, and references therein).

The presence of a geochemical mantle heterogeneity beneath the Azores archipelago is also highlighted by the He isotopic signatures, with high variability in the $^{3}He/^{4}He$ ratios, which show from primitive to more radiogenic values across the different islands (e.g., Jean-Baptiste et al., 2009; Moreira et al., 1999; 2012; Madureira et al., 2014). More primitive $^{3}He/^{4}He$ values (9 to 11.4 *R/Ra*) were measured in rock samples from Terceira Island by Madureira et al. (2005). Lavas from easternmost part of S. Miguel Island showed $^{3}He/^{4}He$ ratios much more radiogenic (*R/Ra* < 5.55) compared with the MORB value (*R/Ra* ~ 8) (Moreira et al., 1999; 2012). Distinct $^{3}He/^{4}He$ ratios were also measured in the S. Miguel (5.23 - 6.07 Ra) and Terceira (12.79 and 13.53 *Ra*) water and gas emissions by Jean-Baptiste et al. (2009), which were in agreement with data measured in the volcanic rocks.

Due to the particular geodynamic setting, seismicity and volcanism occur frequently in the Azores archipelago. Indeed, since their settlement in the 15th century, about 30 volcanic eruptions and several destructive seismic events have affected the islands (Silveira et al., 2003). The present-day volcanic activity is characterized by seismicity and deformation episodes (Trota, 2008; Silva et al., 2012), and by the presence of fumarolic fields, thermal and CO_2-rich springs, and diffuse degassing areas (Viveiros et al., 2010). The main fumarolic emissions are associated with the hydrothermal systems of the active central volcanoes of the S. Miguel, Terceira and Graciosa

Islands (Ferreira et al., 2005). The present study focuses on the main fumaroles of the S. Miguel and Terceira Islands, which show the highest outlet temperatures, at around 100 ºC.

S. Miguel Island is the biggest island of the archipelago, and it has fumarolic emissions associated with the Fogo and Furnas polygenetic caldera volcanoes. Three sub-Plinian eruptions occurred in these areas in historical times: two at Furnas Volcano (1439-43 and 1630; Booth et al., 1978; Cole et al., 1995; Queiroz et al., 1995), and one at Fogo Volcano (1563; Wallenstein et al., 2005). Most of the hydrothermal manifestations at Furnas Volcano are located inside the caldera, where there are three main fumarolic fields (Fig. 1). On the south flank of the Furnas Volcano there are several gas emissions, along the Ribeira Quente Valley and at Ribeira Quente village (Ferreira and Oskarsson, 1999). The degassing structures of the Furnas Volcano are essentially aligned with NW-SE and WNW-ESE trends (Viveiros et al., 2010). In the case of the Fogo volcanic system, the main hydrothermal manifestations are located on the northern flank of the volcano, and these are associated with the NW-SE fault system that defines the so-called Ribeira Grande graben (Carmo et al. 2013).

Furnas do Enxofre is the only fumarolic field of Terceira Island, and it is located in a trachytic dome emplaced where the NW-SE basaltic ridge intersects Pico Alto Volcano. The only volcanic eruption that has taken place in historical times on Terceira Island occurred in 1761 (Self, 1976).

Very few gas and isotopic compositions are available in the literature for the Azorean fumaroles. The first gas analyses available for the S. Miguel fumaroles date from the early 1980's, and these were carried out in the scope of the Azores geothermal program (Truesdell et al., 1984). The fluids that were analysed showed typical hydrothermal origins, with CO_2 representing more than 93% of the dry phase, which has also been confirmed by more recent studies (Ferreira and Oskarsson, 1999; Ferreira et al., 2005). Gas geothermometers applied to the Fogo fumarolic emissions indicated temperatures between 209 °C and 240 °C (Truesdell et al., 1984). The measured reservoir temperatures of the Ribeira Grande geothermal field that is located on the north

flank of Fogo Volcano were given by Carvalho et al. (2006), who showed that these reached 230 °C to 245 °C at depths between 800 m and 1300 m. Despite a deeper and slightly colder aquifer, the geothermal wells also exploit a two-phase aquifer, with a steam fraction of up to 0.081, and a shallower aquifer that is strongly steam enriched. In the case of the Furnas fumaroles, gas thermometers have suggested temperatures from 194 °C to 248 °C (Truesdell et al., 1984). More recent studies have proposed aquifer temperatures of 160 °C to 180 °C at a depth of less than 200 m for the Furnas hydrothermal system, which were based on gas/water thermometry and the deuterium-oxygen isotope shift (Cruz et al., 1999; Ferreira and Oskarsson, 1999).

Although there has been a general characterization of the gases emitted by the Furnas do Enxofre fumaroles (Pico Alto volcano, Terceira Island) (Ferreira et al., 2005), there are no comprehensive geochemical studies available in the literature for this hydrothermal system. A recent geothermal exploration program was undertaken for the central part of Terceira Island, which comprised the drilling of four wells down to 600 m. The temperatures measured revealed a convective zone of at least 233 °C, with interpolated temperatures of between 200 °C and 220 °C for the Furnas do Enxofre area (Henneberger et al., 2004).

In the present study, we provide for the first time a complete dataset of the chemical and isotopic compositions of fumarolic fluids collected at the main fumarolic fields of S. Miguel and Terceira Islands. We used an analytical technique that allowed the simultaneous determination of the Ar, O_2, N_2, CH_4, He, H_2 concentrations and the $\delta^{15}N$ and $^{40}Ar/^{36}Ar$ ratios on a single gas sample, which avoided possibly different sample contamination during multi-injection gas analyses. These analytical data are presented and discussed, to investigate the thermodynamic conditions of the hydrothermal systems, and the origin of the discharged fluids and their relationships with the peculiar geodynamic assessment of this region. Moreover, in the framework of the volcanic surveillance of the Azores Islands, the data obtained in the present study can be used as a reference to highlight possible future compositional changes that are related to variations in the activities of the Furnas, Fogo and Pico Alto volcanoes.

2. Materials and methods

Nine fumaroles with boiling temperatures (96-100 °C) were sampled between September 19 and October 4, 2013 (Fig. 1), with a total number of 11 samples, as the Caldeiras da Ribeira Grande and RG4 fumaroles (samples 6 and 8) were the replicate of samples 5 and 7, collected a week later.

For determination of the major gas species, the fumarolic gases were collected in 200 ml evacuated flasks that contained approximately 50 ml 4 N NaOH solution (Giggenbach, 1975; Giggenbach and Goguel, 1989). In addition, condensed steam and noncondensable gases (dry gas) were separated by passing the fumarolic gases through a water-cooled condenser, with the collection of condensate in 30 ml high-density polyethylene bottles, and of the noncondensable gases in 20 ml glass bottles equipped with two stopcocks.

The chemical and isotopic analyses of the fumarolic effluents were carried out on the NaOH samples at the Laboratory of the *Istituto Nazionale di Geofisica e Vulcanologia, Sezione di Napoli, Osservatorio Vesuviano* (INGV-OV), using a Finnigan Delta plusXP continuous flow mass spectrometer coupled with a gas chromatograph (Agilent Technologies 6890N). The gas chromatograph included two channels equipped with two six-port injection valves, two PLOT columns (MolSiev, 5Å; 30 m × 0.53 mm × 50 μm; He and Ar as carrier gases) and thermal conductivity detectors. He and H_2 were measured on the first channel with Ar as the carrier gas, while the other gas species were analyzed on the second channel, where a post-column switching device allowed the column gas flow to be split to the thermal conductivity detectors, for the determination of the Ar, O_2, N_2 and CH_4 concentrations, and via an open split to the mass spectrometer. In addition, the 2nd channel is equipped with a pre-column (MolSiev, 5Å; 3 m × 0.53 mm × 50 μm) and a supplementary six-port valve, which was used to back-flush the pre-column, to vent undesirable gas species (mainly CO and water), thus preventing these from reaching the mass spectrometer and avoiding the need for column back-flushing, while also reducing the analytical time. To allow simultaneous determination of ^{36}Ar and $\delta^{15}N$, the mass spectrometer was equipped

with a universal triple collector. At the beginning of the measurement, this was set up to focus the ion beam of mass 36 on the more sensitive cup: after the recording of the mass 36 peak, the magnetic field was fast switched to focus the ion beams of masses 28, 29 and 30 on the three cups using a Jump calibration procedure that took into account the hysteresis of the magnet. The partial pressure of each gas species was determined with reference to standards (air, pure gases and calibrated mixture) injected at different pressures. The value of 298.6 was assumed to be the $^{40}Ar/^{36}Ar$ ratio of the air (Lee et al., 2006). This instrumental set-up allowed determination of the $^{40}Ar/^{36}Ar$ ratio and the Ar, O_2, N_2, CH_4, He and H_2 concentrations in a single gas injection, and also of $\delta^{15}N$ [$\delta^{15}N = R_{sample}/R_{ATMosphere}$ -1; $R = (^{14}N^{15}N)/^{14}N_2$] on the same aliquot of gas sample (analytical errors: $\delta^{15}N$ ±0.1‰; concentrations of ^{36}Ar <1%, and ^{40}Ar, O_2, N_2, CH_4, He and H_2 <3%). This is a new analytical procedure of the INGV-OV Laboratory that allows better investigation of the origins of gases that have been potentially affected by air contamination (i.e., N_2, Ar) and represents an improvement of the technique recently used in the analysis of the Yellowstone fumaroles (Chiodini et al., 2012).

The CO_2 and S species absorbed in the alkaline solution were analyzed after their oxidation with H_2O_2, using acid-base titration and ion chromatography, respectively (analytical error, ±3%). Due to the reaction in alkaline solution to form $COOH^-$ (Giggenbach and Matsuo, 1991), CO was analyzed on dry gas samples by gas chromatography separation with a PLOT column (MolSiev 5 Å, 30 m × 0.53 mm × 50μm; He as carrier gas) coupled to a high-sensitivity reduced gas detector (HgO; detection limit, 0.05 ppm).

The isotopic analyses of oxygen and hydrogen of the condensates were performed with a near infrared laser analyzer (Picarro L2130i) using the wavelength-scanned cavity ring down spectroscopy technique (analytical errors: δD ±0.5‰, $\delta^{18}O$ ±0.08‰; data reported vs. Vienna Standard Mean Ocean Water, V-SMOW). Isotopic analyses of the C and O of CO_2 were performed using a mass spectrometer technique on the dry gas samples following gas chromatographic

separation, using the GasBench II device (analytical errors: $\delta^{18}O$ ±0.08‰, $\delta^{13}C$ ±0.06‰; data reported vs. V-SMOW for oxygen, and vs. V-PDB (Vienna Pee Dee Belemnite) for carbon).

The isotopic composition of He ($^3He/^4He$) was determined on the dry gas samples at the INGV Laboratories of Palermo, using a Helix SFT-GVI mass spectrometer, following the method described by Inguaggiato and Rizzo (2004). The data are reported as *R/Ra* values (*Ra*, He isotopic ratio in the atmosphere, as 1.39×10^{-6}; Ozima and Podosek, 2002) corrected for the atmospheric contamination of the sample on the basis of its $^4He/^{20}Ne$ ratio (Sano and Wakita, 1985).

The locations and chemical and isotopic compositions of the samples are reported in Figure 1 and Table 1.

3. Results and discussions

3.1. Gas composition

The main component of all of the fumarolic fluids was H_2O, followed by CO_2, which ranged from 3.1 vol% to 6.7 vol% (Table 1). The concentrations of the other gases were highly variable: in ppmv, H_2S varied from 11 to 322, H_2 from 54 to 347, CH_4 from 1.1 to 185, N_2 from 50 to 185, Ar from 1.1 to 3.9, He from 0.3 to 1.0 and CO from 0.02 to 0.195. The presence of a trace of O_2 reflects minor air contamination during either sampling or storage, or naturally in the sampled vents. The $^{40}Ar/^{36}Ar$ ratios ranged from 299, which is close to the atmospheric value, up to 479.

The carbon isotopic composition of the fumarolic CO_2 was expressed in the δ notation per mil *vs.* V-PDB, and it was relatively constant at S. Miguel ($\delta^{13}C$ -3.94‰ ±0.17‰), within the range of previous measurements (-3.3‰ to -6.1‰; Ferreira and Oskarsson, 1999), while it was more depleted in ^{13}C at Terceira ($\delta^{13}C$ -4.59‰ ±0.1‰). Similarly, the He isotopic composition (expressed as *R/Ra*) was constant for S. Miguel Island, with a range from 5.21 to 5.35, while the Terceira fumarolic fluids were characterized by a different signature that was richer in ^3He with value of ~9.60.

3.2. Gas equilibria: temperature–pressure geoindicators

Reactive and redox-sensitive gas species such as CO, H_2 and CH_4 can potentially reflect the temperature-pressure conditions in a hydrothermal environment. Chiodini and Marini (1998) reviewed hydrothermal gas equilibria in the H_2-CO_2-CO-CH_4-H_2O system with a comparison of analytical data from numerous worldwide hydrothermal systems with theoretical compositions of both equilibrium vapor and equilibrium liquid phases, and the compositions of the vapor phases separated in a single-step from the liquids at varying temperatures. In their approach, which was based on the assumption that all of the gases are in thermodynamic equilibrium, the fugacity of water, f_{H2O}, was controlled by the co-existence of vapor and liquid, and expressed by the T-f_{H2O} relation for pure water (Giggenbach, 1980), as:

$$\text{Log } f_{H2O} = 5.51 - 2048/T\ (K) \quad (1)$$

The assumption of pure water is supported by the relatively low salinity fluids (<0.06 m NaCl) generally encountered in geothermal wells on S. Miguel (Truesdell et al., 1984).

The equilibrium conditions can be adequately described by the two redox-independent reactions given in equations (2) and (3) (Chiodini and Marini, 1998):

$$CO_2 + H_2 \Leftrightarrow CO + H_2O \quad (2)$$

$$3CO_2 + CH_4 \Leftrightarrow 4CO + 2H_2O \quad (3)$$

Assuming that the ratios of the fugacity coefficients Γ_{H2}/Γ_{H2O}, Γ_{CO}/Γ_{CO2}, and $\Gamma_{CH4}/\Gamma_{CO2}$ do not deviate significantly from unity in the typical pressure-temperature range of hydrothermal systems,

the equilibrium constants of equations (2) and (3) can be expressed as in equations (4) and (5), respectively (Chiodini and Marini, 1998):

$$\log(X_{CO}/X_{CO2}) - \log(X_{H2}/X_{H2O}) = -2248/T(K) + 2.485 \quad (4)$$

$$3\log(X_{CO}/X_{CO2}) + \log(X_{CO}/X_{CH4}) = -13727/T(K) + 8.585 \quad (5)$$

Equations (4) and (5) hold for the equilibrated vapor phase (Fig. 2, vapor line), whereas the liquid composition (Fig. 2, liquid line) was computed assuming that the gas species distribute between the vapor and liquid phases according to the distribution coefficients, B_i (Giggenbach, 1980; Chiodini and Marini, 1998). The liquid and the vapor lines delimit the field of vapor produced by boiling processes. In particular, the single-step vapor separation (SSVS) lines in Figure 2 represent the composition of the vapor that is generated from liquids by single-step vapor separation processes at different original temperatures, T_o (see Chiodini and Marini, 1998, for further details).

All of the samples plot within the field delimited by the liquid and vapor curves, which suggests a possible equilibrium condition in the H_2-CO_2-CO-CH_4-H_2O gas system of the fumarolic fluids. In particular, the samples approach the line of pure vapor, which indicates reservoir temperatures from 260 °C to 280 °C for the Fogo samples. Sample#6 is the sole exception to this (the duplicate of sample #5, from Caldeiras de Ribeira Grande on 26/09/13), which indicates a lower temperature of ~190 °C. These estimated temperatures are 30 °C to 35 °C higher than the temperature range measured in the geothermal wells in the area (230-245 °C; Carvalho et al., 2006). Equilibrium temperatures from 200 °C to 275 °C are inferred for the samples collected in the Furnas caldera, which is in agreement with temperature estimates of 200 °C to 250 °C by water and gas geothermometers in earlier studies (Truesdell et al., 1984), and higher than estimations based on the gas/water geothermometry and the deuterium-oxygen isotope shift (Cruz et al., 1999; Ferreira and Oskarsson, 1999). Finally, equilibrium temperatures of approximately 190 °C are inferred for

258 the hydrothermal area of Furnas de Enxofre on Terceira Island, which are quite comparable to the
259 values (from 200 to 220 ºC) extrapolated for the area by Henneberger et al. (2004).

260 Gas equilibria were further investigated following the method of Chiodini and Marini
261 (1998), which consists of the derivation of the fugacities of the gas species at equilibrium
262 temperatures computed on the basis of the T_o, and s (s = fraction of vapor separated during
263 isenthalpic boiling) derived from Figure 2 (see Chiodini and Marini, 1998, for further details).

264 Gas fugacities are useful to assess both redox condition (expressed as $R_H = \log f_{H2}/f_{H2O}$,
265 Giggenbach 1987) and the hydrothermal reactions controlling CO_2 fugacity. In Fig. 3a the S.
266 Miguel and Terceira R_H estimations are compared with (i) relevant redox buffers of the
267 hydrothermal (D'Amore and Panichi, 1980 and FeO-$FeO_{1.5}$ Giggenbach 1987) and volcanic
268 environments (H_2S-SO_2, Giggenbach 1987) and (ii) with similar R_H values inferred for many
269 hydrothermal and volcanic systems (Chiodini and Marini, 1998). Terceira samples fall in the main
270 cluster of hydrothermal systems along the D'Amore and Panichi (1980) relation, while, at S.
271 Miguel, the R_H values correlate with the equilibrium temperatures (according to the empirical
272 function $R_H = -8.19/T - 2.08$; S. Miguel buffer; Fig. 3a) suggesting relatively oxidizing redox
273 conditions that are consistent with those that characterize the hydrothermal systems of active
274 volcanoes in a quiescent state (Fig. 3a).

275 Finally, the computed CO_2 fugacities for the S. Miguel and Terceira fumarolic fluids are
276 plotted against the equilibrium temperatures in Figure 3b, together with the 'full equilibrium'
277 function of Giggenbach (1984, 1988) and the f_{CO2}-temperature functions constrained by typical
278 thermometamorphic reactions. The Azores samples plot close to the 'full equilibrium' conditions,
279 which suggests that their f_{CO2} values are controlled by mineral-solution reactions consisting of the
280 conversion of Ca-Al-silicates to calcite typical of active hydrothermal systems (e.g. Giggenbach,
281 1984).

282

283 ***3.3. Ar, N_2, He and CO_2 compositions***

Unlike the reactive gas species, the inert gases (He, Ar), the near-inert species (N_2) and the main component CO_2 of fumarolic effluents can be used as indicators of the primary provenance of the fluids (Giggenbach, 1996). These gas species were used by Giggenbach and Goguel (1989), Giggenbach (1992), and Giggenbach and Poreda (1993) to characterize the origins of volatile components in relation to tectonic settings. Following the same approach, in the He-Ar-N_2 triangular diagram of Figure 4, most of the samples (1, 4, 6, 7, 8) plot close to the He corner, which would indicate either mantle or crustal origins, whereas the other samples show compositions that are variably contaminated by air and/or air-saturated water (ASW).

Further information on the potential sources of the gases can be furnished by the relative compositions of He isotopes and CO_2. In the ternary diagram involving CO_2, ^3He and ^4He (Fig. 5) the fumarolic samples form two clusters of points. One cluster is represented by the Terceira samples characterized by a plume-like composition with high $^3He/^4He$ ratio (~ 9.60 *R/Ra*) and $CO_2/^3He$ ratio of $7.2 \pm 0.8 \times 10^9$, while the S. Miguel samples with lower $^3He/^4He$ ratios from 5.21 to 5.35 *R/Ra* and higher $CO_2/^3He$ ratio of $10.1 \pm 0.9 \times 10^9$ form the second group. The compositions of S. Miguel fumaroles are similar to the data reported in previous studies (Moreira et al., 1999; Jean-Baptiste et al., 2009), while for Terceira fluids higher $^3He/^4He$ (13.5 *R/Ra*) and $CO_2/^3He$ ratio of $22 \pm 4 \times 10^9$ were reported (Jean-Baptiste et al., 2009). In the diagram of Figure 5 the fumarolic samples can be explained as mixture of a plume-like high $^3He/^4He$ component, represented by the Terceira fluids, and crustal gases enriched in both radiogenic He and limestone derived CO_2, presumably originated from a recycled crustal component. According to this mixing model, S. Miguel samples show an addition of approximately 45% of radiogenic He and ~30% of crustal CO_2 with respect to Terceira samples.

The same mixture is highlighted by the diagrams of $CO_2/^3He$ and $CO_2/^4He$ vs. Carbon isotopic composition expressed as $\delta^{13}C$ (Figs. 6a, b). In the inset of Figure 6a the data are reported on a full scale diagram together with the end-members of MORB, marine limestone and organic sediment (Sano and Marty, 1995). The lines describe mixing models between a high $CO_2/^3He$

plume-like mantle composition, as highlighted in Figure 5 and the end-members of limestone and organic sediment. The plume-like samples of Terceira show the more negative $\delta^{13}C$ values (-4.59 ±0.1‰,), the lowest $CO_2/^3He$ ratios (Fig. 6a) and the highest $CO_2/^4He$ ratios (Fig. 6b). The samples of S. Miguel plot along the mixture lines between the Terceira data and the crustal component characterized by a more positive carbon isotopic composition (^{13}C enriched), a higher $CO_2/^3He$ ratios (because of the addition of limestone derived CO_2), and a lower $CO_2/^4He$ ratios because of the addition of radiogenic He.

A possible origin of this recycled crustal component was proposed by Moreira et al. (2012), who hypothesized a source that contained undegassed material enriched in U and Th, which might be represented by underplated magma that has intruded into the oceanic lithosphere and was subducted (Elliot et al., 2007), and that has been stored in the mantle for the last ~3 Ga. This recycled crustal component could also explain why high CO_2/He ratios are found in the Azores volatile compositions.

Seismic tomography of the region show negative anomalies of seismic velocity beneath the Azores confined in the upper 200-250 km (Yang et al., 2006, Silveira et al., 2006, 2010), but also present at depths as high as 450 km, suggesting the presence of a large deep-derived plume at the origin of the Azores hotspot (e.g., Silveira et al., 2010). Moreover, recent oxygen isotopic compositions (Genske et al., 2013) as well as data from melt inclusions (Métrich et al., 2014) argue for a quite homogeneous mantle source beneath the Azores islands that shows some variability due to intramantle processes and to a minor extent, as in the case of S. Miguel Island, a limited contribution from recycled low-temperature components..

3.3.1. The N_2, ^{36}Ar ^{40}Ar and ^4He compositions

Further information on the potential sources of the gases for S. Miguel Island is given by the $^{40}Ar/^{36}Ar$ ratio, which was used to infer the origin of the inert gas species using the method described in Chiodini et al. (2012). The relevant gas ratios were plotted against the $^{40}Ar^*/^{40}Ar$ ratio;

i.e., the ratio between non-atmospheric Ar ($^{40}Ar^*$) and total ^{40}Ar. The $^{40}Ar^*$ is computed assuming that all of the ^{36}Ar is atmosphere derived ($^{40}Ar^* = {}^{40}Ar - {}^{40}Ar/{}^{36}Ar_{atmosphere} \times {}^{36}Ar_{sample}$, $^{40}Ar/^{36}Ar_{atmosphere} = 298.6$; Lee et al., 2006). An advantage of the use of the $^{40}Ar^*/^{40}Ar$ ratio is that a deep atmosphere-free source is characterized by the value of 1.0 in the ideal case of a ^{36}Ar-free deep component. More realistically, considering the $^{40}Ar/^{36}Ar$ ratios proposed for mantle sources by Marty and Dauphas (2003a), the variable $^{40}Ar^*/^{40}Ar$ would be characterized by values of 0.99 and 0.94 for the upper mantle ($^{40}Ar/^{36}Ar$, 30,000 ±10,000) and mantle plume sources ($^{40}Ar/^{36}Ar$, 5,000 ±1,000), respectively.

Figure 7 shows the $^{40}Ar^*/^{40}Ar$ ratios vs. the $^{40}Ar^*/N_2$ and He/Ar ratios for both the S. Miguel and Terceira fumarolic fluids. In Figure 7, the samples define the mixing trends from atmospheric-like compositions toward deep, atmosphere-free, presumably magmatic component that we assume to be characterized by a $^{40}Ar/^{36}Ar$ of 5,000. This assumption will not imply significant errors for the estimated compositions of the magmatic component (see below), at least for original $^{40}Ar/^{36}Ar$ ratios >5,000.

Although, a relatively wide range in the helium isotopic compositions was measured in groundwater and thermal water in these two islands, attributed to a variable inputs of radiogenic helium to aquifers during water–rock interactions (Jean-Baptiste et al., 2009), our fumarolic data show little or no variation of $^{3}He/^{4}He$ ratios in each system. Consequently, the absence of correlation of He and Ar isotopes (e.g. $^{3}He/^{4}He$ vs. $^{40}Ar/^{36}Ar$), suggests (for S. Miguel samples) that the possible addition of radiogenic He should occur prior to interaction with the hydrothermal environment, maybe at the source level (magmatic). Accordingly, the variability of Ar isotopes could be attributed to a variable mixture of the deep component (that we refer as magmatic component) with an atmospheric-like component.

For the S. Miguel systems, the compositions of the two end-members in the mixing process, the atmospheric component (AC) and the magmatic component (MC), were estimated using the Nonlinear Least Squares Method to fit the data with a model of mixing between the two

components. The computation was restricted to only the S. Miguel system, because at Terceira there were too few samples for this statistical approach, and because the three samples showed the highest amounts of the atmospheric component, which makes the extrapolation of the composition of the magmatic component challenging. The calculations resulted in an atmospheric component composition characterized by $N_2/^{40}Ar$ of 42 ± 3 (1σ) and $^4He/^{40}Ar$ of 0.24 ± 0.16. The estimated $N_2/^{40}Ar$ was close to that of the ASW ($N_2/^{40}Ar$, ~39), while the He-based ratios suggested the addition of small amounts of He, to the ASW (i.e., some He flux would affect the groundwaters involved). The estimated composition of the magmatic component was characterized by $N_2/^{40}Ar$ of 62 ± 6 (i.e., $^{40}Ar^*/N_2$, 1.53×10^{-2}) and $^4He/^{40}Ar$ of 1.02 ± 0.5. This relatively low $^4He/^{40}Ar$ ratio, of which approximately 45% of He could be radiogenic (see section 3.3), suggests a relatively unfractionated magmatic source.

The possible mantle sources are further investigated by the $N_2/^{40}Ar$ vs. $^{40}Ar/^{36}Ar$ diagram (Fig. 8). The estimated $N_2/^{40}Ar$ ratio (62 ± 6) for the magmatic component, even if possibly contaminated by crustal derived fluids, is lower than that expected for the upper mantle fluids (MORB, $N_2/^{40}Ar$, 152 ± 58; Cartigny et al., 2001 and references therein), being compatible with a plume-like composition ($N_2/^{40}Ar$, 74 ± 30; Marty and Dauphas, 2003a).

3.3.2. Nitrogen isotopes

The nitrogen isotope composition of fumarolic fluids varies from $\delta^{15}N$ -3.3‰ to -0.5‰ for S. Miguel fumaroles and from $\delta^{15}N$ -2.4‰ to -1.9‰ for Terceira (Table 1), which are more depleted in ^{15}N with respect to previously published nitrogen isotope data for the Azores fumarolic gases (Grassa et al., 2010): S. Miguel, from $\delta^{15}N$ -2.5‰ to -1.6‰; Terceira, from $\delta^{15}N$ -0.7‰ to -0.3‰.

Following the approach of Fischer et al. (2002), in Figure 9, the N isotopes and the N_2/He values are compared with possible pure and mixed end-members (air, ASW, mantle and

subduction-related material). The method implicitly assumes that N_2 and He are not fractionated by magmatic or hydrothermal processes (Fischer et al., 2002).

Samples from S. Miguel are compatible with a main mantle composition that was variably contaminated by both ASW and fluids, possibly derived from subducted material. Up to 65% of the nitrogen would derive from the mantle source on the assumption of the typical mantle end-member isotopic composition ($\delta^{15}N$, -5‰; Marty et al., 1996).

The samples from Terceira are out of the mixing field among these three end-members, which suggests either the occurrence of N-fractionation processes or a mantle fluid characterized by $\delta^{15}N$ values more negative than the typical upper-mantle signature (Fig. 9, Terceira mixing? line). The presence of a source with such negative isotopic signatures would suggest its origin from the deep mantle, where very negative $\delta^{15}N$ values have been hypothesized on the basis of the nitrogen isotopic composition of diamonds (Boyd et al., 1987; Boyd and Pillinger, 1988; 1994; Javoy et al., 1984; Cartigny et al., 1997; Palot et al., 2012).

Based on the above discussion, the samples of S. Miguel might also derive from a mantle source more depleted in ^{15}N than that typical of the mantle (Fig. 9, dashed lines), thus more readily explaining the $\delta^{15}N$ - $N_2/^{36}Ar$ relationships in the samples analyzed (Fig. 10). In Figure 10, only the mixing of a ^{15}N-depleted mantle composition with air (or ASW) would fully explain the position of all of the samples, including the Terceira gases. The position of the S. Miguel data might suggest the same mantle source with the addition of greater amounts of air than at Terceira (Fig. 10), or more likely, of crustal-derived fluids, as highlighted by the $N_2/^4He$ ratios (Fig. 9) and CO_2-^3He-^4He relative compositions (Fig. 4). Using an Ar-N isotope mass balance, as described in Grassa et al. (2010), the isotopic composition of the atmosphere-free N_2 can be inferred to be $\leq$ -14‰ at Terceira, and $\leq$ -9‰ at S. Miguel. This mass-balance, is based on the assumption of ASW ($N_2/^{36}Ar$ = 1.15×10^4) as an atmospheric proxy and it is very sensitive to air contamination, even if it is low, resulting in a more positive $\delta^{15}N$ estimate. For this reason, although most of the samples show low air contamination, these estimated values should be considered as the most ^{15}N enriched

413 composition possible for the mantle end-member. For example, if we consider as an atmospheric
414 proxy the estimated atmospheric component (AC, $N_2/^{40}Ar = 42$; $N_2/^{36}Ar = 1.25 \times 10^4$), the possible
415 $\delta^{15}N$ mantle compositions result to be of ~ - 11‰ at S. Miguel and of ~ -23 ‰ at Terceira.

416 Moreover, the possible unique mantle source for Terceira and S. Miguel fumarolic data is
417 highlighted in Figure 11, where nitrogen isotopes are reported vs. the $N_2/^3He$ ratios, together with
418 the mixing lines among the possible end-members, air or ASW, crustal derived fluids (Sano et al.,
419 2001) and a possible Azores mantle composition. In this picture, S. Miguel samples are compatible
420 with the same mantle source of Terceira with the addition of approximately 45-55 % (excluding
421 atmospheric components) of crustal derived Nitrogen.

422 Although the source and evolution of the nitrogen in the mantle is still debated (Cartigny
423 and Ader, 2003; Marty and Dauphas, 2003a, b; Kerrich and Jia, 2004; Cartigny and Marty, 2013),
424 currently nitrogen derived from the upper mantle shows a $\delta^{15}N$ of -5 ±1‰ (Marty et al., 1996),
425 while the ocean island basalt samples (OIB), from the lower mantle reservoirs, indicate modern
426 plumes that are more positive ($\delta^{15}N$ >0‰) (Marty et al., 1998; Dauphas and Marty, 1999; Marty
427 and Dauphas, 2003a; Mohapatra et al., 2009). However, the occurrence of ^{15}N-depleted lower
428 mantle regions is supported by studies of diamonds from different localities and origins (Boyd et
429 al., 1987; Boyd and Pillinger, 1988, 1994) and in particular those of Zaire (Javoy et al., 1984),
430 Fuxian (China; Cartigny et al., 1997), and Kankan (Guinea; Palot et al., 2012), the primordial
431 nitrogen signature of which ($\delta^{15}N$ <-30‰) has been inferred for deep mantle regions. In this light,
432 the nitrogen isotopic compositions of the sampled fumarolic fluids are in agreement with the
433 presence of deep mantle regions that have been preserved from homogenisation (with the
434 primordial N_2 signature retained) during deep-mantle convection, crustal extraction and slab
435 recycling (Palot et al., 2012).

436 To sum up, with the exclusion of chemical or isotopic gas fractionation that involved N
437 during shallow secondary processes, nitrogen with an isotopic composition ($\delta^{15}N$, ≤-14‰) that is
438 significantly more depleted in ^{15}N than those typical of the upper mantle ($\delta^{15}N$, -5 ±1‰; Marty et

al., 1996) and modern plumes ($\delta^{15}N$ >0‰; Marty et al., 1998; Dauphas and Marty, 1999; Marty and Dauphas, 2003a; Mohapatra et al., 2009) can be inferred for the Azores mantle source. A similar nitrogen isotopic composition was reported for the fumarolic fluids from the Hengill area in southwest Iceland, with a mantle plume composition characterized by $N_2/^{40}Ar$ of 60 ±20 and $\delta^{15}N$ of -10.4 ±0.2‰ (Marty et al., 1991).

3.5. Origins of the water

The isotopic compositions of the steam condensates from the fumarolic fluids ranged for oxygen from $\delta^{18}O$ of -8.5‰ to -5.6‰, and for deuterium from δD of -39.3‰ to -22.4 ‰. Significant steam condensation processes at near discharge conditions appear not to affect the fumarolic fluids sampled, as shown by the positive relationship of δD (and also $\delta^{18}O$) vs. CO_2 concentrations. This positive relationship holds also for the He concentrations, and it is opposite to what would be expected for condensation processes.

These analytical values in the classical $\delta^{18}O$ vs. δD diagram of Figure 12 plot on the left side of the diagram very far from the isotopic composition of the meteoric water line, which makes the interpretation of the possible origins a challenge. Chiodini et al. (2000) demonstrated that oxygen exchange between CO_2 and steam in fumarolic fluids is fast enough to allow rapid isotopic re-equilibration across a wide temperature range (100-1000 °C), showing that the measured $\delta^{18}O_{CO2}$ and $\delta^{18}O_{H2O}$ of fumarolic vapor collected from five different volcanic and hydrothermal systems are very close to the theoretical fractionation (Richet et al., 1977) expected for oxygen exchange between these two gaseous molecules at the discharge temperatures. Upon cooling of the gas, the increasing oxygen isotopic fractionation between CO_2 and H_2O progressively depletes the steam in the heavier isotope component, whereas the $\delta^{18}O$ composition of the whole H_2O+CO_2 gas system remains constant regardless of the temperature. Accordingly, the origin of the water component of fumaroles is investigated here by considering the role of oxygen isotope exchange between H_2O and CO_2 in the gas phase. The computed $1000\times\ln\alpha_{CO2\text{-}H2O}$ of the S. Miguel and Terceira fumarolic

fluids are reported against the discharge temperatures in Figure 13, together with the data from several fumarolic systems worldwide (Chiodini et al., 2000) and the theoretical curve for the equilibrium fractionation between CO_2 and H_2O in the gas phase (Richet et al., 1977). The agreement of these Azores data with both the theoretical fractionation factor and the behavior of the other fumarolic systems suggests that oxygen re-equilibration is also an active process in the Azores fumaroles, and might lead to interpretative bias.

Figure 12 illustrates the analytical steam isotopic compositions, together with the average local meteoric water (δD, -20‰; $\delta^{18}O$, -4 ‰; IAEA, 1992) and the global meteoric water line (Craig, 1961). Moreover, Figure 12 shows the modeling of the two most important secondary processes that affect the isotopic composition of geothermal fluids during their rise to the surface; i.e., steam separation due to adiabatic decompression of the thermal fluids, and mixing with shallow groundwaters (Giggenbach and Stewart, 1982). In particular, in these models, the oxygen re-equilibration between CO_2 and H_2O in the gas phase at varying temperatures is also considered. Starting from a liquid at 300 °C (close to the maximum temperature of gas equilibria), the two models were computed considering the different CO_2 contents in the gas phase (from 0% to 7%, which covered the range of the analytical data). The gas phase that results from the iso-enthalpic single-step steam separation process and the equilibrium vapor that results from the mixing of the hydrothermal liquid with the groundwaters (at 20 °C) are then cooled to the fumarolic discharge temperature (~100 °C), and are reported as the isotopic compositions of the steam in Figure 12. In general, all of the sampled fumarolic fluids are in agreement with these fractionation models, which suggest the presence of a parent-liquid that is characterized by δD of ~ -25‰ and $\delta^{18}O$ of ~ -3.0‰. This parent-liquid composition applies to all of the measured fumarolic samples overall, and it suggests a mainly meteoric origin that was possibly modified by water-rock ^{18}O exchange at high temperatures. It is worth noting that the inferred parent-liquid isotopic composition is close to the liquid compositions measured in geothermal wells drilled in the Fogo area (Truesdell et al., 1984).

4. Conclusions

Analytical data from the S. Miguel and Terceira Islands are presented and discussed here to provide a comprehensive picture of the thermodynamic conditions of their hydrothermal systems. For S. Miguel Island, the gas geoindicators suggest reservoir temperatures ranging from 190 °C to 280 °C for the Fogo hydrothermal system, as temperatures that are 30 °C to 35 °C as maximum values higher than those measured for geothermal wells and available in the literature (230 - 245 °C; Carvalho et al., 2006). Temperatures as high as 280 °C have been estimated for the reservoir that feeds the RG4 fumarolic field that developed close to a disused geothermal well from 2010. The equilibrium temperatures estimated for the Furnas hydrothermal system vary from 200 °C to 275 °C, and these are in relative agreement with the estimation of 200 °C to 250 °C for water and gas geothermometry (Truesdell et al., 1984). For S. Miguel, the gas equilibria in the H_2-CO_2-CO-CH_4-H_2O system suggest hydrothermal system redox conditions that are more oxidizing than those typical for hydrothermal environments (i.e., FeO-$FeO_{1.5}$, and DP redox buffers), similar to the most-oxidizing conditions already identified for hydrothermal systems (Chiodini and Marini, 1998). This suggests an immature hydrothermal environment, where the presence of magmatic and more oxidizing fluids prevents attainment of the typical hydrothermal redox conditions (Giggenbach, 1993). On the other hand, the chemical compositions of the fumarolic fluids discharged on Terceira Island indicate equilibrium vapor at a temperature of ~ 190 °C along with the typical redox conditions of DP buffer.

The He isotopic composition of ~9.6 *R/Ra* measured in the fumaroles of Terceira and the *R/Ra* values of up to 13.5 measured in phenocrysts and fluids (Jean-Baptiste et al., 2009, and references therein), suggest a plume-like composition presumably from a lower mantle source.

The relative compositions of He isotopes and CO_2 suggest for S. Miguel fluids an origin from a mixture of a plume-like high $^3He/^4He$ component, represented by the Terceira fluids, and crustal fluids enriched in both radiogenic He and limestone derived CO_2, presumably originated from a recycled crustal component. According to this mixing model, S. Miguel samples show an addition

517 of approximately 45% of radiogenic He and ~30% of crustal CO_2 with respect to Terceira samples,
518 thus explaining the relatively low $^3He/^4He$ ratios (from 5.21 to 5.35 *R/Ra*), which is significantly
519 lower than that expected for a mantle origin. This recycled crustal component could also explain
520 why high CO_2/He ratios are found in the Azores volatile compositions.

521 A possible origin of this crustal component was proposed by Moreira et al. (2012), who
522 hypothesized a source that contained undegassed material enriched in U and Th, which might be
523 represented by underplated magma that has intruded into the oceanic lithosphere and was subducted
524 (Elliot et al., 2007), and that has been stored in the mantle for the last ~3 Ga.

525 A mainly meteoric origin of the water, which represents the major component of the
526 fumarolic fluids, can be inferred by its isotopic composition, when taking into account the oxygen
527 isotope exchange between CO_2 and H_2O in the gas phase. Furthermore, the origin of the S. Miguel
528 fumarolic fluids investigated here through the N_2, ^{36}Ar, ^{40}Ar, and ^4He compositions suggests a
529 mixing of an atmospheric-like component and a magmatic component of mantle origin. In
530 particular, the estimated composition for the Atmospheric component ($N_2/^{40}Ar$, 42 ±3; $^4He/^{40}Ar$,
531 0.24 ± 0.16) suggests an ASW origin, with the addition of a small amount of He. The estimated
532 magmatic $^4He/^{40}Ar$ (1.02 ± 0.5) ratio indicates a relatively unfractionated magmatic source, while
533 the $N_2/^{40}Ar$ (62 ± 6) ratio suggests a possible plume-like mantle source. A similar deep component
534 that is characterized by both relatively low $N_2/^{40}Ar$ ratios and negative $\delta^{15}N$ was inferred for the
535 mantle plume feeding the fumarolic fluids in southwest Iceland (i.e., the Hengill area: $N_2/^{40}Ar$, 60
536 ±20; $\delta^{15}N$, -10.4 ±0.2‰; Marty et al., 1991).

537 Nitrogen isotope compositions characterized by very negative $\delta^{15}N$ values ($\delta^{15}N \leq$ -14‰)
538 are inferred for the fluids source of Terceira. Also S. Miguel fluids are compatible with the same
539 source with a possible involvement of crustal-derived Nitrogen. These values are more negative
540 than the typical compositions of both the upper mantle and plume-like mantle, which thus supports
541 the possible presence of a ^{15}N-depleted source, presumably from the lower mantle, in the region.

In conclusion, the present study provides a comprehensive picture of the thermodynamic conditions of the hydrothermal systems of the S. Miguel and Terceira Islands, and it provides new insight for our understanding of the geodynamic context of the Azores archipelago. Furthermore, in the framework of the volcanic surveillance of the Azores, the data obtained in the present study can be used as reference to highlight possible future compositional changes related to variations in the activities of the Furnas, Fogo and Pico Alto volcanoes.

Acknowledgements

The authors thank the AE and two anonymous reviewers for their useful comments that helped to improve the manuscript. This study was financially supported by the European Science Foundation (ESF), in the framework of the Research Networking Programme MeMoVolc. F. Viveiros was supported by a postdoctoral grant from Fundo Regional da Ciência, Região Autónoma dos Açores (PROEMPREGO Operational Program)), and currently is supported by a postdoctoral grant from Fundação para a Ciência e Tecnologia (Ref. SFRH/BPD/100032/2014). A. L. Rizzo and the INGV Laboratories of Palermo are acknowledged for the $^{3}He/^{4}He$ analyses.

References

Barry P. H., Hilton D. R., Fischer T. P., de Moor J. M., Mangasini F., and Ramirez C. (2013) Helium and carbon isotope systematics of cold "mazuku" CO_2 vents and hydrothermal gases and fluids from Rungwe Volcanic Province, southern Tanzania. *Chem. Geol.* **339**, 141-156. doi:10.1016/j.chemgeo.2012.07.003.

Bonatti E. (1990) Not so hot “hot spots” in the oceanic mantle. *Science* **250**, 107-111.

Booth B., Croasdale R., and Walker G. P. L. (1978) A quantitative study of five thousand years of volcanism on Sao Miguel, Azores. *Philosophical Transactions of the Royal Society of London. Series A, Mathematical and Physical Sciences* **288**, 271-319.

Boyd S. R., Mattey D. P., Pillinger C. T., Milledge H. J., Mendelssohn M., and Seal M. (1987) Multiple growth events during diamond genesis: an integrated study of carbon and nitrogen

isotopes and nitrogen aggregation state in coated stones. *Earth Planet. Sci. Lett.* **86**, 341-353.

Boyd S. R. and Pillinger C. T. (1988) Carbon and nitrogen isotopes in the mantle. *Chem. Geol.* **70**, 46.

Boyd S. R. and Pillinger C. T. (1994) A preliminary study of $^{15}N^{14}N$ in octahedral growth form diamonds. *Chem. Geol.* **116**, 43-59.

Burnard P., Stuart F., and Turner G. (1994) C-He-Ar variations within a dunite nodule as a function of fluid inclusion morphology. *Earth Planet. Sci. Lett.* **128**, 243-258.

Cannat M., Briais A., Deplus C., Escartín J., Georgen J., Lin J., Mercouriev S., Meyzen C., Muller M., and Pouliquen G. (1999) Mid-Atlantic Ridge–Azores hotspot interactions: along-axis migration of a hotspot-derived event of enhanced magmatism 10 to 4 Ma ago. *Earth Planet. Sci. Lett.* **173**, 257-269.

Carmo R., Madeira J., Hipólito A., and Ferreira T. (2013) Paleoseismological evidence for historical surface faulting in São Miguel island (Azores). *Ann. Geophys.* **56**, S0671.

Cartigny P. and Ader M. (2003) A comment on "The nitrogen record of crust–mantle interaction and mantle convection from Archean to Present" by B. Marty and N. Dauphas [Earth Planet. Sci. Lett. 206 (2003) 397–410]. *Earth Planet. Sci. Lett.* **216**, 425-432.

Cartigny P. and Marty B. (2013) Nitrogen Isotopes and Mantle Geodynamics: The Emergence of Life and the Atmosphere–Crust–Mantle Connection. *Elements* **9**, 359–366. doi: 10.2113/gselements.9.5.359

Cartigny P., Boyd S., Harris J., and Javoy M. (1997) Nitrogen isotopes in peridotitic diamonds from Fuxian, China: the mantle signature. *Terra Nova* **9**, 175-179.

Cartigny P., Jendrzejewski N., Pineau F., Petit E., and Javoy M. (2001) Volatile (C, N, Ar) variability in MORB and the respective roles of mantle source heterogeneity and degassing: the case of the Southwest Indian Ridge. *Earth Planet. Sci. Lett.* **194**, 241-257.

Carvalho M. R., Forjaz V. H., and Almeida C. (2006) Chemical composition of deep hydrothermal fluids in the Ribeira Grande geothermal field (São Miguel, Azores). *J. Volcanol. Geotherm. Res.* **156**, 116-134.

Chiodini G., Allard P., Caliro S., and Parello F. (2000) ^{18}O exchange between steam and carbon dioxide in volcanic and hydrothermal gases: implications for the source of water. *Geochim. Cosmochim. Acta* **64**, 2479-2488.

Chiodini G., Caliro S., Lowenstern J. B., Evans W. C., Bergfeld D., Tassi F., and Tedesco D. (2012) Insights from fumarole gas geochemistry on the origin of hydrothermal fluids on the Yellowstone Plateau. *Geochim. Cosmochim. Acta* **89**, 265–278. doi: 10.1016/j.gca.2012.04.051.

Chiodini G. and Marini L. (1998) Hydrothermal gas equilibria: The H_2O-H_2-CO_2-CO-CH_4 system. *Geochim. Cosmochim. Acta* **62**, 2673-2687.

Cole P. D., Queiroz G., Wallenstein N., Gaspar J. L., Duncan A. M., and Guest J. E. (1995) An historic subplinian/phreatomagmatic eruption: the 1630 AD eruption of Furnas volcano, Sa˜o Miguel, Azores. *J. Volcanol. Geotherm. Res.* **69**, 117-135.

612 Craig H. (1961) Isotopic variations in meteoric waters. *Science* **133**, 1702-1703.

613 Cruz J. V., Coutinho R. M., Carvalho M. R., Oskarsson N., and Gislason S. R. (1999) Chemistry of
614 waters from Furnas volcano, São Miguel, Azores: fluxes of volcanic carbon dioxide and
615 leached material. *J. Volcanol. Geotherm. Res.* **92**, 151-167.

616 D'Amore F. and Panichi C. (1980) Evaluation of deep temperatures of hydrothermal systems by a
617 new gas geothermometer. *Geochim. Cosmochim. Acta* **44**, 549-556.

618 Dauphas N. and Marty B. (1999) Heavy nitrogen in carbonatites of the Kola Peninsula: A possible
619 signature of the deep mantle. *Science* **286**, 2488-2490.

620 Elliott T., Blichert-Toft J., Heumann A., Koetsier G., and Forjaz V.-H. (2007) The origin of
621 enriched mantle beneath São Miguel, Azores. *Geochim. Cosmochim. Acta* **71**, 219–240.

622 Ferreira T., Gaspar J. L., Viveiros F., Marcos M., Faria C., and Sousa F. (2005) Monitoring of
623 fumarole discharge and CO_2 soil degassing in the Azores: contribution to volcanic
624 surveillance and public health risk assessment. *Ann. Geophys*. **48**, 787-796

625 Ferreira T. and Oskarsson N. (1999) Chemistry and isotopic composition of fumarole discharges of
626 Furnas caldera. *J. Volcanol. Geotherm. Res.* **92**, 169-179.

627 Fischer T. P., Hilton D. R., Zimmer M. M., Shaw A. M., Sharp Z. D., and Walker J. A. (2002)
628 Subduction and recycling of nitrogen along the Central American margin. *Science* **297**,
629 1154-1157.

630 Genske F.S., Beier C., Haase K.M., Turner S.P., Krum, S., and Brandl P.A. (2013) Oxygen isotopes
631 in the Azores islands: Crustal assimilation recorded in olivine. *Geology* **41**, 491-494.

632 Gente P., Dyment J., Maia M., and Goslin J. (2003) Interaction between the Mid-Atlantic Ridge and
633 the Azores hot spot during the last 85 Myr: Emplacement and rifting of the hot spot-derived
634 plateaus. *Geochem. Geophys. Geosys.* **4**, 8514. doi:10.1029/2003GC000527.

635 Giggenbach W. F. (1975) A simple method for the collection and analysis of volcanic gas samples.
636 *Bull.Volcanol.* **39**, 132-145.

637 Giggenbach W. F. (1980) Geothermal gas equilibria. *Geochim. Cosmochim. Acta* **44**, 2021-2032.

638 Giggenbach W. F. (1984) Mass transfer in hydrothermal alteration systems—a conceptual
639 approach. *Geochim. Cosmochim. Acta* **48**, 2693-2711.

640 Giggenbach W. F. (1987) Redox processes governing the chemistry of fumarolic gas discharges
641 from White Island, New Zealand. *Appl. Geochem.* **2**, 143-161.

642 Giggenbach W. F. (1988) Geothermal solute equilibria. Derivation of Na-K-Mg-Ca geoindicators.
643 *Geochim. Cosmochim. Acta* **52**, 2749.

644 Giggenbach W. F. (1992) The composition of gases in geothermal and volcanic systems as a
645 function of tectonic setting. *Proceedings - International Symposium on Water-Rock*
646 *Interaction* **7,** 873-878.

647 Giggenbach W. F. (1993) Redox control of gas compositions in Philippine volcanic-hydrothermal
648 systems. *Geothermics* **22**, 575-587.

649 Giggenbach W. F. (1996) Chemical composition of volcanic gases. In *Monitoring and Mitigation of*
650 *Volcano Hazards* (eds. R. Scarpa and R. I. Tilling). Springer, pp. 221–256.

651 Giggenbach W. F. and Goguel R. L. (1989) Collection and analysis of geothermal volcanic water
652 and gas discharges. Chemistry Division, DSIR, New Zealand. Report no. CD 2401.

653 Giggenbach W. F. and Matsuo S. (1991) Evaluation of results from Second and Third IAVCEI field
654 workshops on Volcanic gases, Mt. Usu, Japan, and White Island, New Zealand. *Appl.*
655 *Geochem.* **6**, 125-141.

656 Giggenbach W. F. and Poreda R. J. (1993) Helium isotopic and chemical composition of gases from
657 volcanic-hydrothermal systems in the Philippines. *Geothermics* **22**, 369-380.

658 Giggenbach W.F., Sano Y., and Wakita H., (1993). Isotopes of He, and CO_2 and CH_4 contents in
659 gases produced along the New Zealand part of a convergent plate boundary. *Geochim.*
660 *Cosmochim. Acta* **57**, 3427–3455. doi:10.1016/0016-7037(93)90549-C.

661 Giggenbach W. F. and Stewart M. K. (1982) Processes controlling the isotopic composition of
662 steam and water discharges from steam vents and steam-heated pools in geothermal areas.
663 *Geothermics* **11**, 71.

664 Graham D. W. (2002) Noble gas isotope geochemistry of mid-ocean and ocean island basalts:
665 characterization of mantle source reservoirs. *Rev. Mineral. Geochem.* **47**, 247-317.
666 doi:10.2138/rmg.2002.47.8.

667 Grassa F., Capasso G., Oliveri Y., Sollami A., Carreira P., Carvalho M. R., Marques J. M., and
668 Nunes J. C. (2010) Nitrogen isotopes determination in natural gas: analytical method and
669 first results on magmatic, hydrothermal and soil gas samples. *Isot. Environ. Health Stud.* **46**,
670 141-155. doi:10.1080/10256016.2010.491914.

671 Henneberger R., Cabeças R., Martins R., and Granados E. (2004) Pico Alto, Terceira: a new
672 geothermal field in the Azores. *Geoth. Res. T.*, 28.

673 Hipólito A., Madeira J., Carmo R., and Gaspar J. L. (2013) Neotectonics of Graciosa island
674 (Azores): a contribution to seismic hazard assessment of a volcanic area in a complex
675 geodynamic setting. *Ann. Geophys.* **56**, S0677.

676 IAEA. (1992) International Atomic Energy Agency (IAEA). Statistical treatment of environmental
677 isotope data in precipitation. Technical Reports Series No. 331, IAEA, Vienna (1992), p.
678 255, pp.

679 Inguaggiato S. and Rizzo A. (2004) Dissolved helium isotope ratios in ground-waters: a new
680 technique based on gas-water re-equilibration and its application to Stromboli volcanic
681 system. *Appl. Geochem.* **19**, 665-673. doi:10.1016/j.apgeochem.2003.10.009.

682 Javoy M., Pineau F., and Delorme H. (1986) Carbon and Nitrogen isotopes in the mantle. *Chem.*
683 *Geol.* **57**, 41-62.

684 Javoy M., Pineau F., and Demaiffe D. (1984) Nitrogen and carbon isotopic in the diamonds of
685 Mbuji Mayi (Zaire). *Earth Planet. Sci. Lett.* **68**, 399–412.

686 Jean-Baptiste P., Allard P., Coutinho R., Ferreira T., Fourré E., Queiroz G., and Gaspar J. L. (2009)
687 Helium isotopes in hydrothermal volcanic fluids of the Azores archipelago. *Earth Planet.*
688 *Sci. Lett.* **281**, 70-80.

689 Kerrich R. and Jia Y. (2004) A comment on "The nitrogen record of crust–mantle interaction and
690 mantle convection from Archean to Present" by B. Marty and N. Dauphas [Earth Planet. Sci.
691 Lett. 206 (2003) 397–410]. *Earth Planet. Sci. Lett.* **225**, 435-440.

692 Lee J.-Y., Marti K., Severinghaus J. P., Kawamura K., Yoo H.-S., Lee J. B., and Kim J. S. (2006) A
693 redetermination of the isotopic abundances of atmospheric Ar. *Geochim. Cosmochim. Acta*
694 **70**, 4507-4512. doi:10.1016/j.gca.2006.06.1563.

695 Luis J. F., Miranda J. M., Galdeano A., and Patriat P. (1998) Constraints on the structure of the
696 Azores spreading center from gravity data. *Mar. Geophys. Res.* **20**, 157-170.

697 Madureira P., Moreira M., Mata J., and Allègre C. J. (2005) Primitive neon isotopes in Terceira
698 Island (Azores archipelago). *Earth Planet. Sci. Lett.* **233**, 429-440.

699 Madureira P., Moreira M., Mata J., Nunes J. C., Gautheron C., Lourenço N., Carvalho R., and
700 Abreu M. P. (2014) Helium isotope systematics in the vicinity of the Azores triple junction:
701 Constraints on the Azores geodynamics. *Chem. Geol.* **372**, 62-71.

702 Marty B. (1995) Nitrogen content of the mantle inferred from N_2-Ar correlation in oceanic basalts.
703 *Nature* **377**, 326-328.

704 Marty B. and Dauphas N. (2003a) The nitrogen record of crust-mantle interaction and mantle
705 convection from Archean to present. *Earth Planet. Sci. Lett.* **206**, 397-410.

706 Marty B. and Dauphas N. (2003b) "Nitrogen isotopic compositions of the present mantle and the
707 Archean biosphere": Reply to comment by Pierre Cartigny and Magali Ader. *Earth Planet.*
708 *Sci. Lett.* **216**, 433-439.

709 Marty B., Gunnlaugsson E., Jambon A., Oskarsson N., Ozima M., Pineau F., and Torssander P.
710 (1991) Gas geochemistry of geothermal fluids, the Hengill area, southwest rift zone of
711 Iceland. *Chem. Geol.* **91**, 207.

712 Marty B., Humbert F., and Zimmermann L. (1996) Nitrogen isotopes in oceanic basalt glasses. *27th*
713 *Lunar Planet. Sci. Conf.* pp. 819–820.

714 Marty B. and Jambon A. (1987) C/^{3}He in volatile fluxes from the solid Earth: implication for
715 carbon geodynamics. *Earth Planet. Sci. Lett.* **83**, 16–26.

716 Marty B., Tolstikhin I. N., Kamensky I. L., Nivin V., Balaganskaya E., and Zimmermann L. (1998)
717 Plume-derived rare gases in 380Ma carbonatites from the Kola region (Russia) and the
718 argon isotopic composition in the deep mantle. *Earth Planet.Sci. Lett.* **164**, 179-192.

719 Marty B. and Zimmermann L. (1999) Volatiles (He, C, N, Ar) in mid-ocean ridge basalts:
720 assesment of shallow-level fractionation and characterization of source composition.
721 *Geochim. Cosmochim. Acta* **63**, 3619.

722 Métrich N., Zanon V., Créon L., Hildenbrand A., Moreira M., and Marques F. O. (2014) Is the
723 'Azores Hotspot'a Wetspot? Insights from the Geochemistry of Fluid and Melt Inclusions in
724 Olivine of Pico Basalts. *J. Petrol.* **55**, 377-393.

725 Mohapatra R. K., Schwenzer S. P., Herrmann S., Murty S. V. S., Ott U., and Gilmour J. D. (2009)
726 Noble gases and nitrogen in Martian meteorites Dar al Gani 476, Sayh al Uhaymir 005 and
727 Lewis Cliff 88516: EFA and extra neon. *Geochim. Cosmochim. Acta* **73**, 1505-1522.

728 Moreira M., Doucelance R., Kurz M. D., Dupré B., and Allègre C. J. (1999) Helium and lead
729 isotope geochemistry of the Azores Archipelago. *Earth Planet. Sci. Lett.* **169**, 189-205.

730 Moreira M., Kanzari A., and Madureira P. (2012) Helium and neon isotopes in São Miguel island
731 basalts, Azores Archipelago: New constraints on the "low ^{3}He" hotspot origin. *Chem. Geol.*
732 **322**, 91-98.

733 Moreira M., Kunz J., and Allègre C. J. (1998) Rare gas systematics in popping rock: isotopic and
734 elemental compositions in the upper mantle. *Science* **279**, 1178-1181.
735 doi:10.1126/science.279.5354.1178.

736 Ozima M. and Podosek F. A. (2002) *Noble gas geochemistry*. Cambridge University Press, UK

737 Palot M., Cartigny P., Harris J. W., Kaminsky F. V., and Stachel T. (2012) Evidence for deep
738 mantle convection and primordial heterogeneity from nitrogen and carbon stable isotopes in
739 diamond. *Earth Planet. Sci. Lett.* **357**, 179-193. doi:10.1016/j.epsl.2012.09.015.

740 Queiroz G., Gaspar J. L., Cole P. D., Guest J. E., Wallenstein N., Duncan A. M., and Pacheco J.
741 (1995) Erupções vulcânicas no vale das Furnas (ilha de S. Miguel, Açores) na primeira
742 metade do século XV. *Açoreana* **8**, 159-165.

743 Richet P., Bottinga Y., and Javoy M. (1977) Review of Hydrogen, Carbon, Nitrogen, Oxygen,
744 Sulfur and Chlorine stable isotope fractionation among gaseous molecules. *An. Rev. Earth*
745 *Planet. Sci.* **5**, 65-110.

746 Sano Y. and Marty B. (1995) Origin of carbon in fumarolic gas from island arcs. *Chemical Geology*
747 **119**, 265-274.

748 Sano Y., and Wakita H. (1985) Geographical distribution of ^{3}He/^{4}He in Japan: implications for arc
749 tectonics and incipient magmatism. *J. Geophys. Res.* **90**, 8729–8741.

750 Sano Y., Takahata N., Nishio Y., Fischer T. P., and Williams S. N. (2001) Volcanic flux of nitrogen
751 from the Earth. *Chem. Geol.* **171**, 263.

752 Schilling J. G. (1975) Azores mantle blob: rare-earth evidence. *Earth Planet. Sci. Lett.* **25**, 103-115.

753 Schilling J. G., Bergeron M. B., Evans R., and Smith J. V. (1980) Halogens in the Mantle Beneath
754 the North Atlantic. *Philosophical Transactions of the Royal Society of London. Series A,*
755 *Mathematical and Physical Sciences* **297**, 147-178.

756 Searle R. (1980) Tectonic pattern of the Azores spreading centre and triple junction. *Earth Planet.*
757 *Sci. Lett.* **51**, 415-434.

758 Self S. (1976) The recent volcanology of Terceira, Azores. *J. Geol. Soc.* **132**, 645-666.

759 Silva R., Havskov J., Bean C., and Wallenstein N. (2012) Seismic swarms, fault plane solutions,
760 and stress tensors for São Miguel Island central region (Azores). *J. Seismol.* **16**, 389-407.

761 Silveira D., Gaspar J. L., Ferreira T., and Queiroz G. (2003) Reassessment of the historical seismic
762 activity with major impact on S. Miguel Island (Azores). *Nat. Hazards Earth Syst. Sci.* **3**,
763 615-623.

764 Silveira G, Stutzmann E, Davaille A, Montagner JP, Mendes-Victor L, and Sebai A. (2006) Azores
765 hotspot signature in the upper mantle. *J. Volcanol. Geotherm. Res. 156*, 23-34.

766 Silveira G., Vinnik L., Stutzmann E., Farra V. Kiselev S, and Morais I. (2010) Stratification of the
767 Earth beneath the Azores from P and S receiver function. *Earth Planet. Sci. Lett.* **299**, 91-
768 103.

769 Trieloff M., Kunz J., Clague D. A., Harrison D., and Allégre C. J. (2000) The Nature of pristine
770 noble gases in mantle plumes. *Science* **288**, 1036. doi: 10.1126/science.288.5468.1036.

771 Trota A. (2008) Crustal deformation studies in S. Miguel and Terceira Islands (Azores). Volcanic
772 unrest evaluation in Fogo/Congro area (S. Miguel), University of the Azores.

773 Truesdell A. H., Nehring N. L., and Janik C. J. (1984) Final Report: Geochemical study of thermal
774 fluids from São Miguel Island, Azores, pp. 16

775 Trull T., Nadeau S., Pineau F., Polvé M., and Javoy M. (1993) C-He systematics in hotspot
776 xenoliths: implications for mantle carbon contents and carbon recycling. *Earth Planet. Sci.*
777 *Lett.* **118**, 43-64.

778 Viveiros F., Cardellini C., Ferreira T., Caliro S., Chiodini G., and Silva C. (2010) Soil CO_2
779 emissions at Furnas volcano, São Miguel Island, Azores archipelago: Volcano monitoring
780 perspectives, geomorphologic studies, and land use planning application. *J. Geophys. Res.*
781 **115**, B12208. doi:10.1029/2010JB007555.

782 Wallenstein N., Chester D. K., and Duncan A. M. (2005) Methodological implications of volcanic
783 hazard evaluation and risk assessment: Fogo Volcano, Sao Miguel, Azores. *Zeitschrift für*
784 *Geomorphologie. Supplementband* **140**, 129.

785 Yang T., Shen Y., Van der Lee S., Solomon S. C., and Hung S. H. (2006) Upper mantle structure
786 beneath the Azores hotspot from finite-frequency seismic tomography. *Earth Planet. Sci.*
787 *Lett.* **250**, 11-26.

788

Figure captions

Figure 1. (a) Map showing the location of the Azores archipelago and its main tectonic structures. MAR, Mid-Atlantic Ridge; TR (s.l.), Terceira Rift; C, Corvo; Fl, Flores; F, Faial; P , Pico; SJ, S. Jorge; G, Graciosa; T, Terceira; SM, S. Miguel; (based on Hipólito et al., 2013 and references therein). **(b, c)** Maps showing the sample locations for the S. Miguel (b) and Terceira (c) Islands.

Figure 2. Equilibrium values of log (H_2O/H_2) + log (CO/CO_2) vs. 3log (CO/CO_2) + log (CO/CH_4) in the H_2-CO_2-CO-CH_4-H_2O gas system. The single saturated vapor phase and the single saturated liquid phase are shown as the vapor line and the liquid line, respectively. The composition of single-step vapor separates reflect isenthalpic boiling from T_o to several discrete temperatures (SSVS lines). Vapors separated at constant temperatures (T_s) are also shown. All of the samples plot close to the vapor line at equilibrium temperatures from about 190 °C to 280 °C. The size of the symbols encompasses the estimated errors, also for the following figures.

Figure 3. a) Plot of log (fH_2/fH_2O) vs. equilibrium temperatures. The equilibrium single vapor phase of Terceira and S. Miguel fumaroles, and the computed redox buffer are shown, together with the values of the vapors from geothermal systems (squares, Italian geothermal systems: Larderello, Travale, Amiata, Bagnore) and fumarolic vapors (circles) of hydrothermal systems at quiescent volcanoes (Nisyros, Greece; Vesuvius, Solfatara, Ischia, Italy; Montserrat, West Indies; Guagua Pichincha, Ecuador). Triangles, crater fumarolic fluids of Vulcano Island (data from Chiodini and Marini, 1998); solid lines, FeO-$FeO_{1.5}$ (Giggenbach, 1980), the D'Amore and Panichi (1980) hydrothermal buffers, and the H_2S-SO_2 magmatic gas buffer (Giggenbach, 1987).

b) Plot of f_{CO2} for the equilibrium single saturated vapor phase vs. equilibrium temperatures (after Chiodini and Marini, 1998). The data for the geothermal systems of central Italy (squares) and hydrothermal systems at dormant volcanoes (circles) are shown for comparison. The full

equilibrium function of Giggenbach (1984, 1988) and f_{CO2}-temperature equilibrium values for relevant metamorphic reactions are also shown.

Figure 4. Ternary plot of N_2, He and Ar relative contents of the S. Miguel and Terceira fumaroles. The potential end-member compositions, mantle, arc-type, air and air saturated water are shown for comparison.

Figure 5. Ternary plot of CO_2, ^3He and ^4He relative compositions (after Giggenbach et al., 1993; Barry et al., 2013) of the fumarolic samples. S. Miguel data can be explained as mixture of a plume-like high $^3He/^4He$ component, represented by the Terceira fluids, and crustal derived gases. Terceira high $^3He/^4He$ component is drawn considering R/Ra values from Jean-Baptiste et al., (2009). MORB composition (8±1 *R/Ra*, Graham, 2002; $CO_3/^3He$ $2\pm1 \times 10^9$, Marty and Jambon, 1987) is also reported for comparison.

Figure 6. Diagrams of the $\delta^{13}C$ of CO_2 vs. $CO_2/^3He$ (a) and $CO_2/^4He$ (b) ratios of the fumarolic fluids. In the inset are reported the mixing lines between a high $CO_2/^3He$ composition and the end-members of limestone and organic sediment (Sano and Marty, 1995). In general, the fumarolic fluids are compatible with a mantle origin. In particular, the S. Miguel fluids show a relative increase in radiogenic ^4He and CO_2 that are characterized by a more positive $\delta^{13}C$ value because of the possible addition of crustal derived fluids, with respect to the Terceira fluids. Mantle compositions are also reported: for ocean island basalts (OIB) $\delta^{13}C$ from -7‰ to -4‰ (Javoy et al., 1986), $CO_2/^3He$ of 1-10 $\times 10^9$ and $CO_2/^4He$ of 4-40 $\times 10^4$ (Burnard et al., 1994; Trull et al., 1993); for mid-ocean-ridge basalts (MORB) $CO_2/^3He$ of $2\pm1 \times 10^9$, (Marty and Jambon 1987) and $CO_2/^4He$ of 0.5-7.0 $\times 10^4$ (Marty and Zimmermann, 1999; Trull et al., 1993).

840 **Figure 7.** Diagrams of the He/Ar (a) and Ar*/N_2 (b) ratios vs. Ar*/Ar ratio. In general, the
841 fumarolic samples suggest a mixing between two end-members, with one characterized by an
842 atmospheric-like composition (AC) and the other characterized by a deep atmosphere-free,
843 magmatic composition (MC). The Terceira samples were not used in the estimations of the
844 atmospheric component and the magmatic component, but are reported for comparison.
845
846 **Figure 8.** Diagram of $N_2/^{40}Ar$ ratios vs. the $^{40}Ar/^{36}Ar$ ratios. The estimated S. Miguel magmatic
847 component (MC) suggests a possible plume-like composition of the fluids. Upper and lower mantle
848 fields are roughly estimated from the data available on fluid inclusions. For the mantle plume:
849 $^{40}Ar/^{36}Ar$ and $N_2/^{40}Ar$ ratios from Marty and Dauphas (2003a). For the upper mantle: $^{40}Ar/^{36}Ar$
850 ratios from Moreira et al. (1998) and $N_2/^{40}Ar$ ratios from Cartigny et al., (2001) and references
851 therein.
852
853 **Figure 9.** Diagram of $N_2/^{4}He$ vs. $\delta^{15}N$. The S. Miguel and Terceira hydrothermal fluids are
854 reported, together with possible end-members: air, ASW, mantle and subducted material. The S.
855 Miguel samples are compatible with a mantle origin that has been variably contaminated by both
856 ASW and fluids derived from subducted material. Conversely, although the Terceira fluids suggest
857 a mantle origin, it was probably more depleted in ^{15}N than the upper mantle. The sediment end-
858 member range is from Fischer et al. (2002). The N_2/He ratio of 55 ±30 for the mantle was computed
859 by combining the $N_2/^{40}Ar$ (152 ±58; Cartigny et al., 2001) and $^{4}He/^{40}Ar$ (3 ±1; Marty, 1995) for the
860 upper mantle, together with $N_2/^{40}Ar$ of 74 ±30 (Marty and Dauphas, 2003a) and the $^{4}He/^{40}Ar$ from
861 0.3 to 2.5 (Trieloff et al., 2000) for plume-like mantle composition.
862
863 **Figure 10.** Diagram of the $N_2/^{36}Ar$ vs. $\delta^{15}N$ (after Sano et al., 2001). Nitrogen-Argon isotope
864 relationship suggests a ^{15}N depleted deep source in the Azores. In particular, $\delta^{15}N \leq$-14‰ for
865 Terceira fluids, was inferred by applying the following isotopic mass balance (Grassa et al., 2010):

866 $\delta^{15}N_{deep} = (\delta^{15}N \times N_2)/(N_2 - {}^{36}Ar \times (N_2/{}^{36}Ar)_{ASW})$, where the $N_2/{}^{36}Ar$ ratio of ASW is assumed to be
867 1.15×10^4. Also S. Miguel fluids could be compatible with this source with the addition of greater
868 amounts of air than at Terceira, or more likely, of crustal-derived fluids.
869
870 **Figure 11.** Diagram of the $N_2/{}^3He$ vs. $\delta^{15}N$ (after Sano et al., 2001). The mixing lines among a
871 possible Azores mantle composition, the ASW and Sediments (Sano et al., 2001) are also reported.
872 This possible mantle composition applies to all of the measured fumarolic samples overall. S.
873 Miguel data suggest the addition of approximately 45 -55 % of crustal derived Nitrogen.
874
875 **Figure 12.** Isotopic composition of the fumarolic steam (δD vs. $\delta^{18}O$). Analytical values are
876 reported together with the local meteoric water and global meteoric water line, which is assumed to
877 be represented by the global relation: $\delta D = 8 \times \delta^{18}O + 10$ (Craig, 1961). The two most important
878 secondary processes that might affect rising hydrothermal fluids are also shown: adiabatic steam
879 separation from the hydrothermal liquid (PL) and mixing of this parent liquid with meteoric water
880 (MW). The effects of cooling of the vapors to 100 °C with different CO_2 concentrations are also
881 shown, considering the oxygen isotope exchange between CO_2 and H_2O in the gas phase (see text).
882
883 **Figure 13.** Relationship between the $1000 \times \ln\alpha_{CO2-H2O}$ in the Azores hydrothermal fluids, and their
884 discharge temperature. The polynomial best fit for the fumarolic data from five worldwide
885 fumarolic systems (Chiodini et al., 2000) and the theoretical curve for the equilibrium fractionation
886 between CO_2 and H_2O in the gas phase at the same temperatures (Richet et al., 1977) are shown for
887 comparison. The fumarolic data plot close to the theoretical fractionation line and suggests the
888 attainment of oxygen isotopic equilibrium between CO_2 and steam at the discharges temperatures.
889
890 **Table 1.** Analytical data of the fumarolic fluids sampled. The coordinates refer to WGS84 UTM
891 26S. Chemical compositions are expressed in μmol/mol. Isotopic compositions of C, O and H, and

892 N are expressed in delta notation per mil *vs.* V-PDB, V-SMOW, and Atmosphere, respectively. The
893 He isotopic compositions are expressed as *R/Ra* (with *R* as the $^{3}He/^{4}He$ ratio in the sample, and *Ra*
894 as the $^{3}He/^{4}He$ ratio in the air) corrected for the atmospheric contamination of the sample on the
895 basis of its $^{4}He/^{20}Ne$ ratio (Sano and Wakita, 1985). T_o and T_s (°C) refer to the equilibrium
896 temperature and the vapor-liquid separation temperature, respectively.

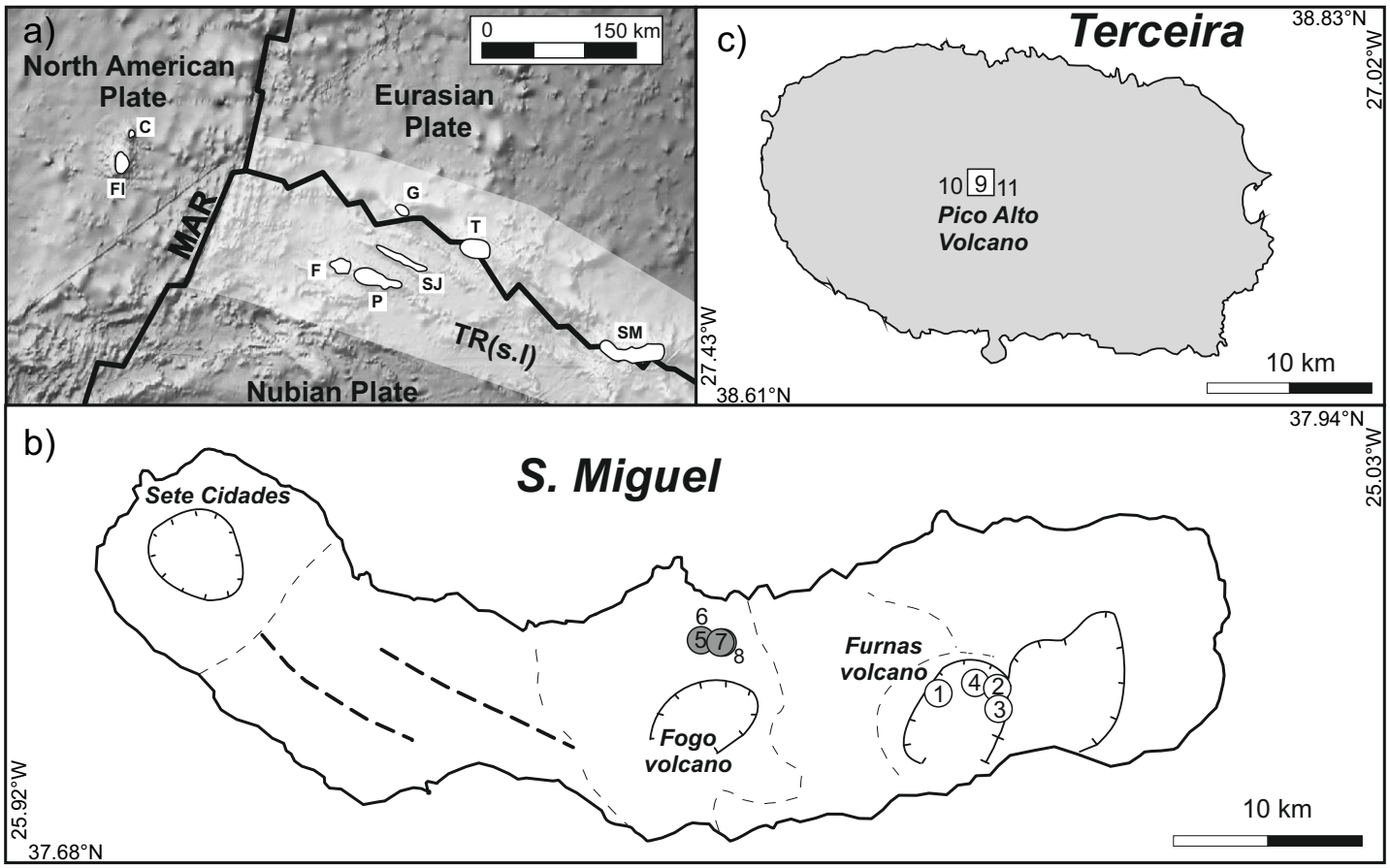
a)
North American Plate
Eurasian Plate
Nubian Plate
0 150 km
C
Fl
MAR
G
T
F
SJ
P
TR(s.l)
SM
c)
Terceira
38.83°N
27.02°W
10 9 11
Pico Alto Volcano
27.43°W
38.61°N
10 km
b)
S. Miguel
37.94°N
25.03°W
Sete Cidades
6
5 7 8
Furnas volcano
1 4 2 3
Fogo volcano
25.92°W
37.68°N
10 km

Figure 1

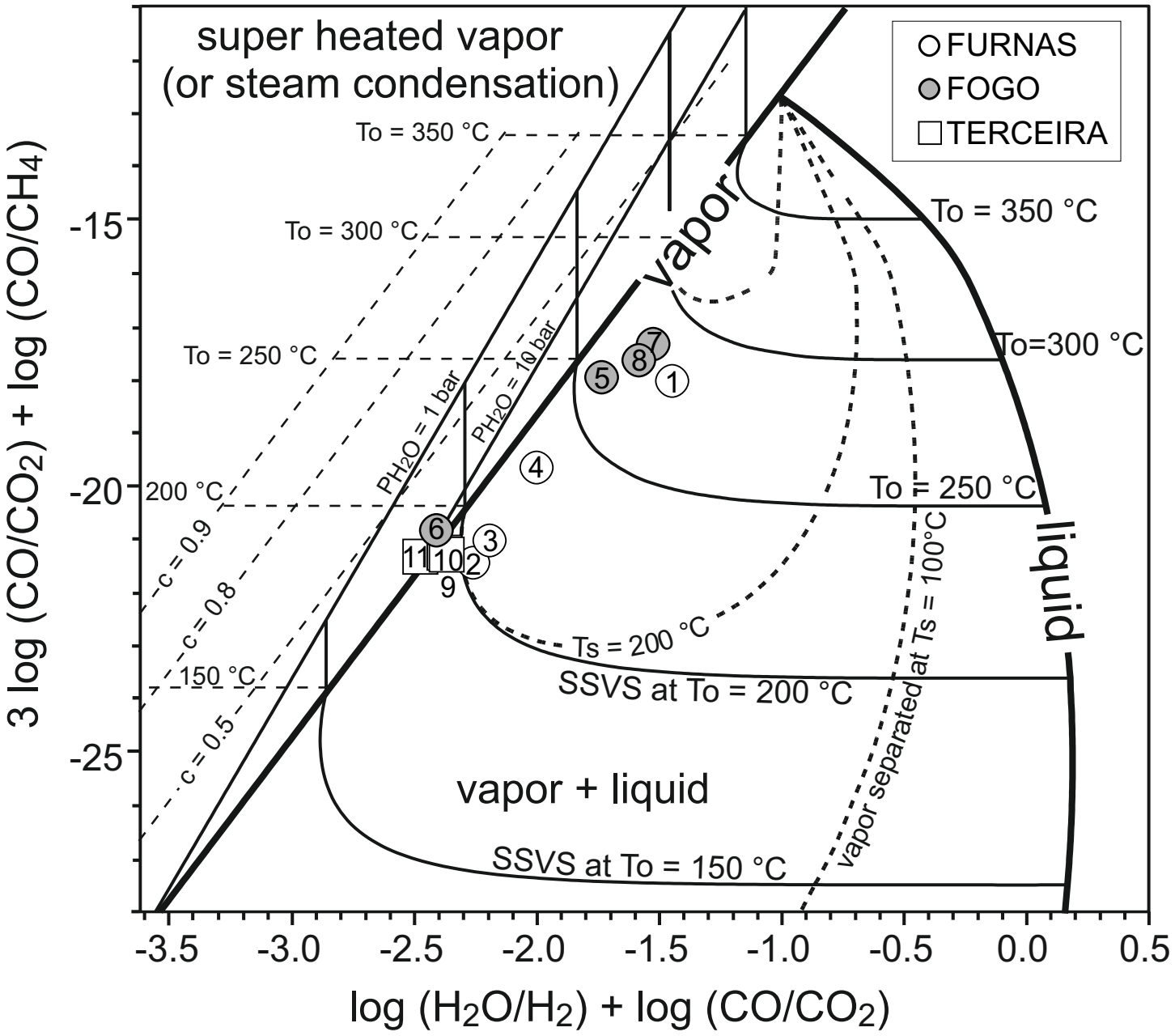
super heated vapor
(or steam condensation)
FURNAS
FOGO
TERCEIRA
To = 350 °C
To = 300 °C
To = 250 °C
200 °C
150 °C
c = 0.9
c = 0.8
c = 0.5
PH2O = 1 bar
PH2O = 10 bar
vapor
liquid
To = 350 °C
To=300 °C
To = 250 °C
Ts = 200 °C
SSVS at To = 200 °C
vapor + liquid
SSVS at To = 150 °C
vapor separated at Ts = 100°C
1
2
3
4
5
6
7
8
9
10
11
-15
-20
-25
-3.5
-3.0
-2.5
-2.0
-1.5
-1.0
-0.5
0.0
0.5
3 log (CO/CO2) + log (CO/CH4)
log (H2O/H2) + log (CO/CO2)

Figure 2

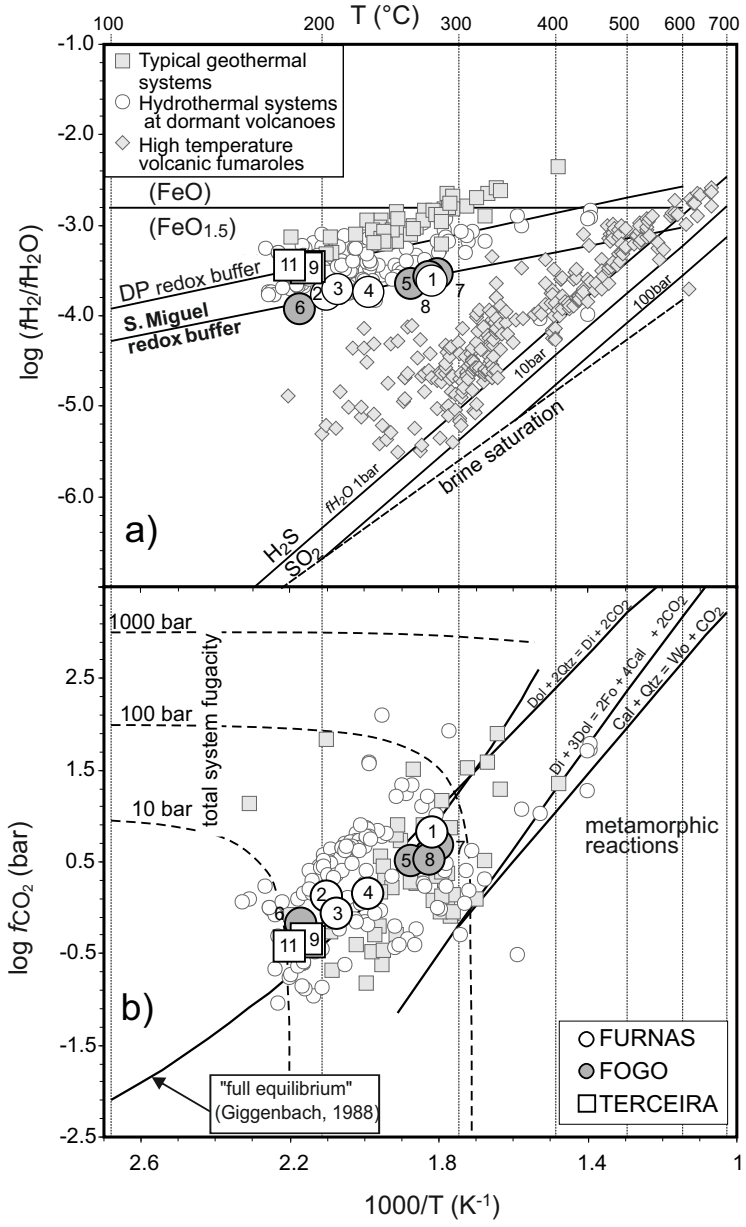
T (°C)
100
200
300
400
500
600
700
Typical geothermal systems
Hydrothermal systems at dormant volcanoes
High temperature volcanic fumaroles
(FeO)
(FeO1.5)
DP redox buffer
S. Miguel redox buffer
log (fH2/fH2O)
a)
fH2O 1bar
H2S
SO2
10bar
100bar
brine saturation
1000 bar
100 bar
10 bar
total system fugacity
log fCO2 (bar)
b)
Dol + 2Qtz = Di + 2CO2
Di + 3Dol = 2Fo + 4Cal + 2CO2
Cal + Qtz = Wo + CO2
metamorphic reactions
"full equilibrium" (Giggenbach, 1988)
FURNAS
FOGO
TERCEIRA
1000/T (K-1)

Figure 3

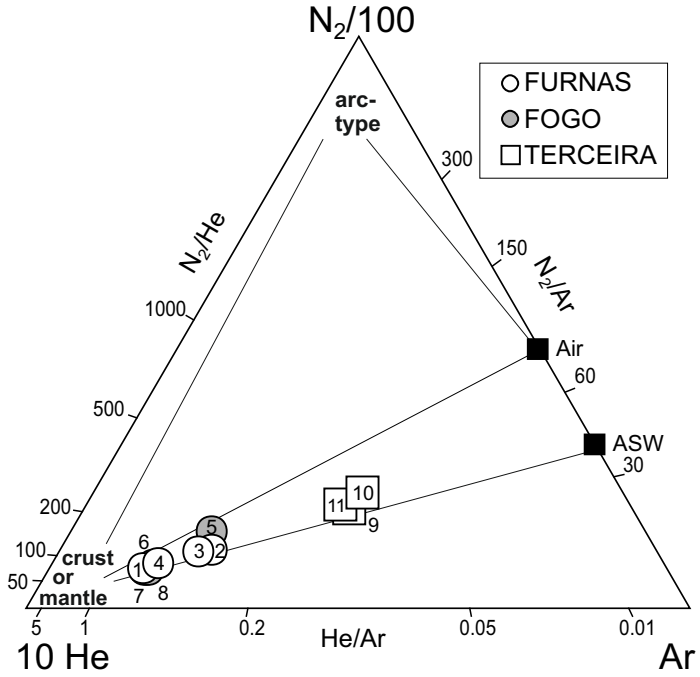
N2/100
FURNAS
FOGO
TERCEIRA
arc-
type
300
150
N2/Ar
N2/He
1000
500
200
100
50
Air
60
ASW
30
crust
or
mantle
1
2
3
4
5
6
7
8
9
10
11
5
1
0.2
He/Ar
0.05
0.01
10 He
Ar

Figure 4

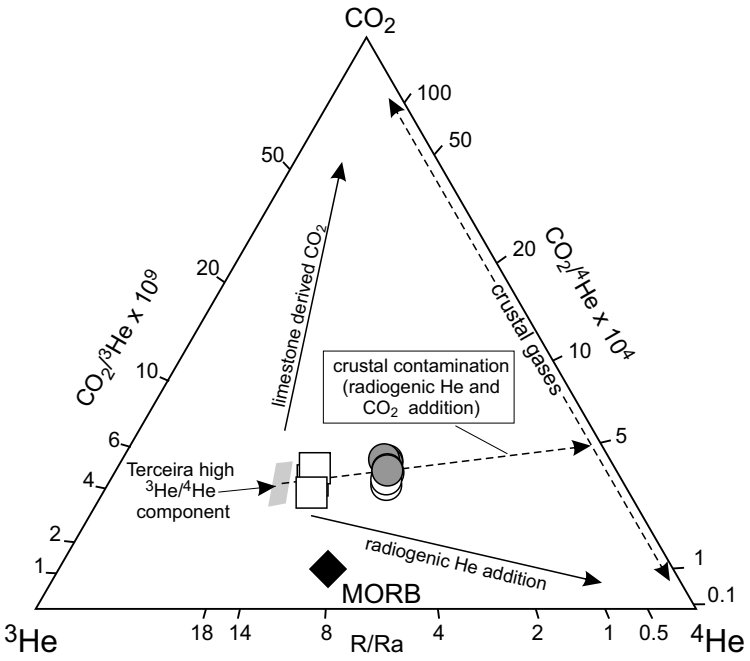
CO2
100
50
20
10
5
1
0.1
50
20
10
6
4
2
1
CO2/3He x 10^9
CO2/4He x 10^4
limestone derived CO2
crustal gases
crustal contamination
(radiogenic He and
CO2 addition)
Terceira high
3He/4He
component
radiogenic He addition
MORB
3He
18 14 8 R/Ra 4 2 1 0.5
4He

Figure 5

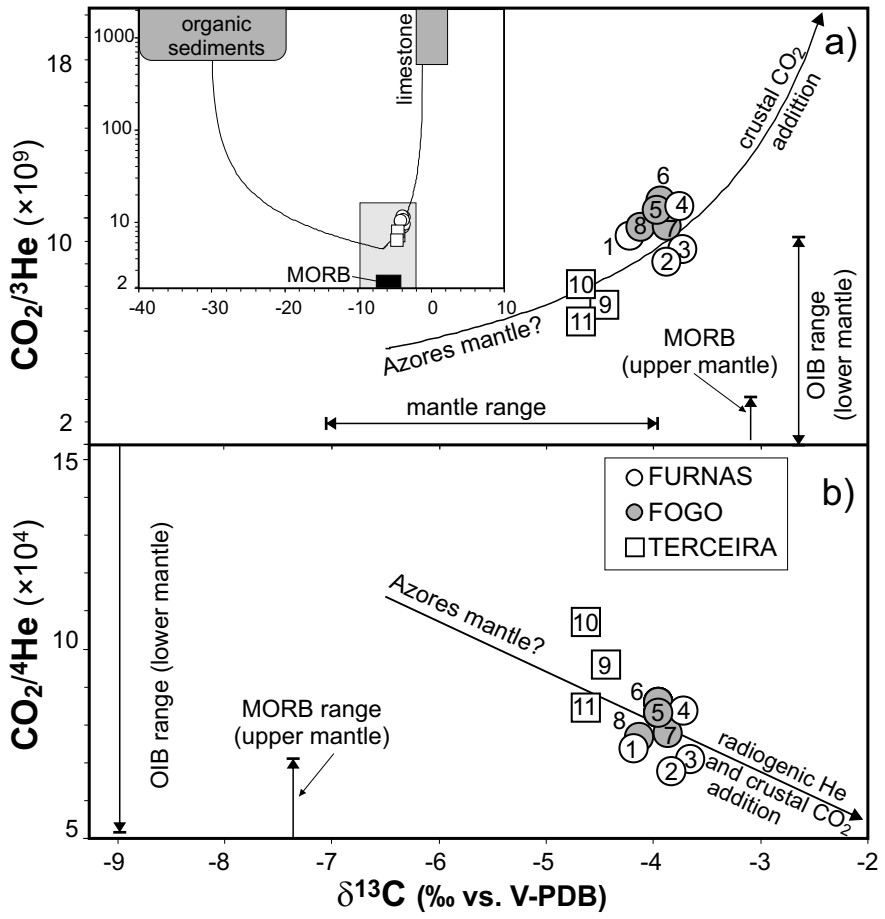
a)
b)
organic sediments
limestone
MORB
crustal CO_2 addition
Azores mantle?
MORB (upper mantle)
mantle range
OIB range (lower mantle)
FURNAS
FOGO
TERCEIRA
MORB range (upper mantle)
radiogenic He and crustal CO_2 addition
$CO_2/^3He$ (×10^9)
$CO_2/^4He$ (×10^4)
$\delta^{13}C$ (‰ vs. V-PDB)

Figure 6

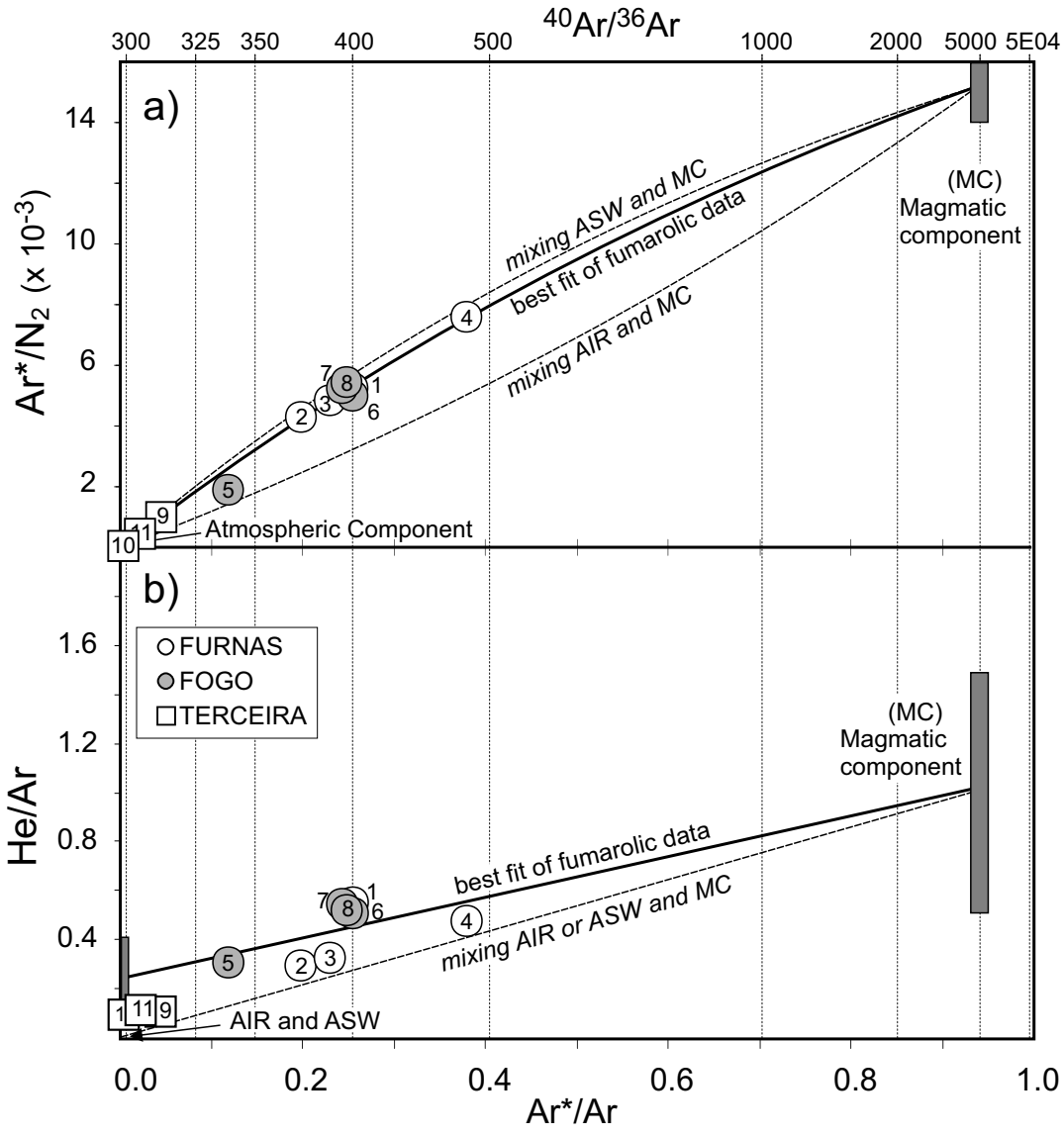
$^{40}Ar/^{36}Ar$
300
325
350
400
500
1000
2000
5000
5E04
a)
Ar^*/N_2 (x 10^{-3})
14
10
6
2
mixing ASW and MC
best fit of fumarolic data
mixing AIR and MC
(MC)
Magmatic
component
Atmospheric Component
b)
FURNAS
FOGO
TERCEIRA
He/Ar
1.6
1.2
0.8
0.4
best fit of fumarolic data
mixing AIR or ASW and MC
(MC)
Magmatic
component
AIR and ASW
0.0
0.2
0.4
0.6
0.8
1.0
Ar*/Ar

Figure 7

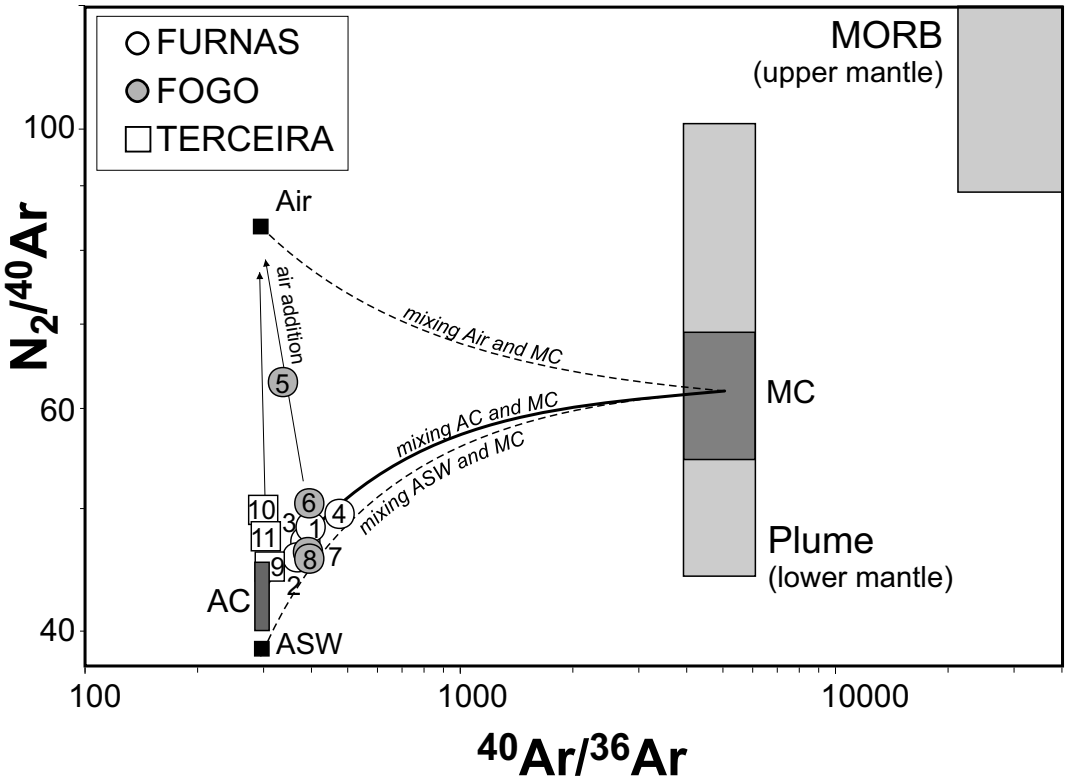
FURNAS
FOGO
TERCEIRA
MORB
(upper mantle)
Air
air addition
mixing Air and MC
mixing AC and MC
mixing ASW and MC
MC
Plume
(lower mantle)
AC
ASW
100
60
40
100
1000
10000
N2/40Ar
40Ar/36Ar

Figure 8

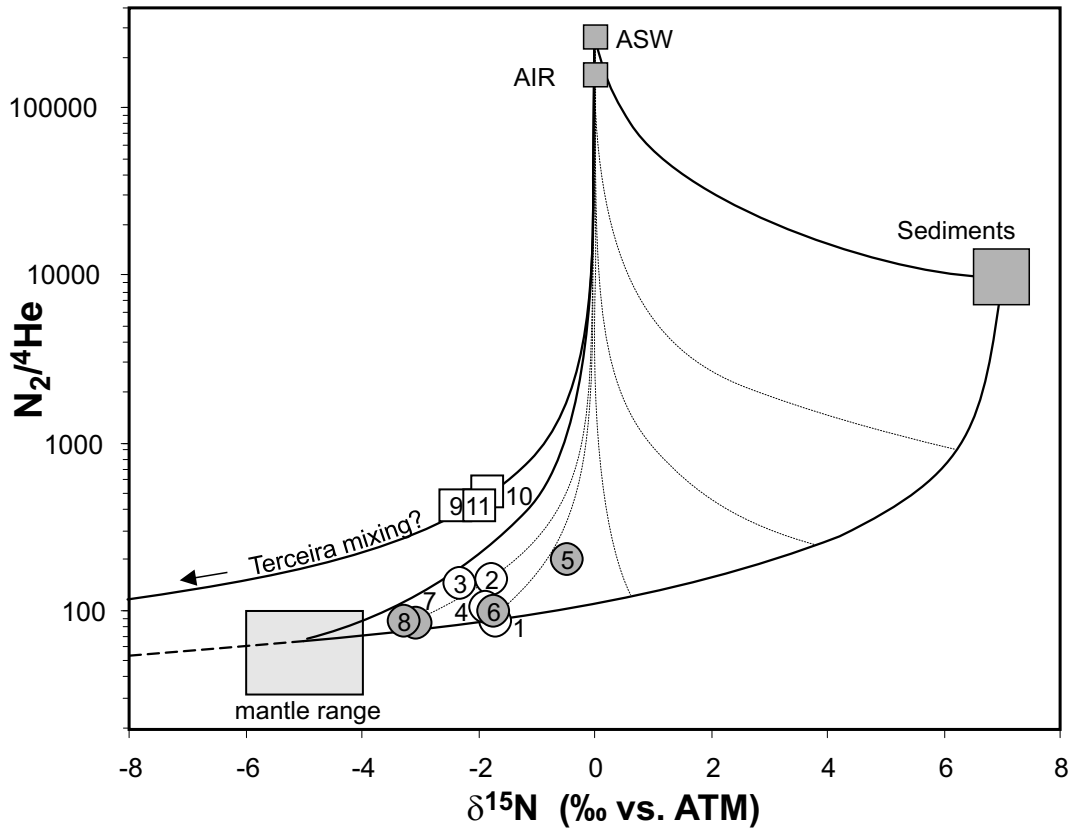
ASW
AIR
Sediments
Terceira mixing?
mantle range
100000
10000
1000
100
-8
-6
-4
-2
0
2
4
6
8
N2/4He
δ15N (‰ vs. ATM)

Figure 9

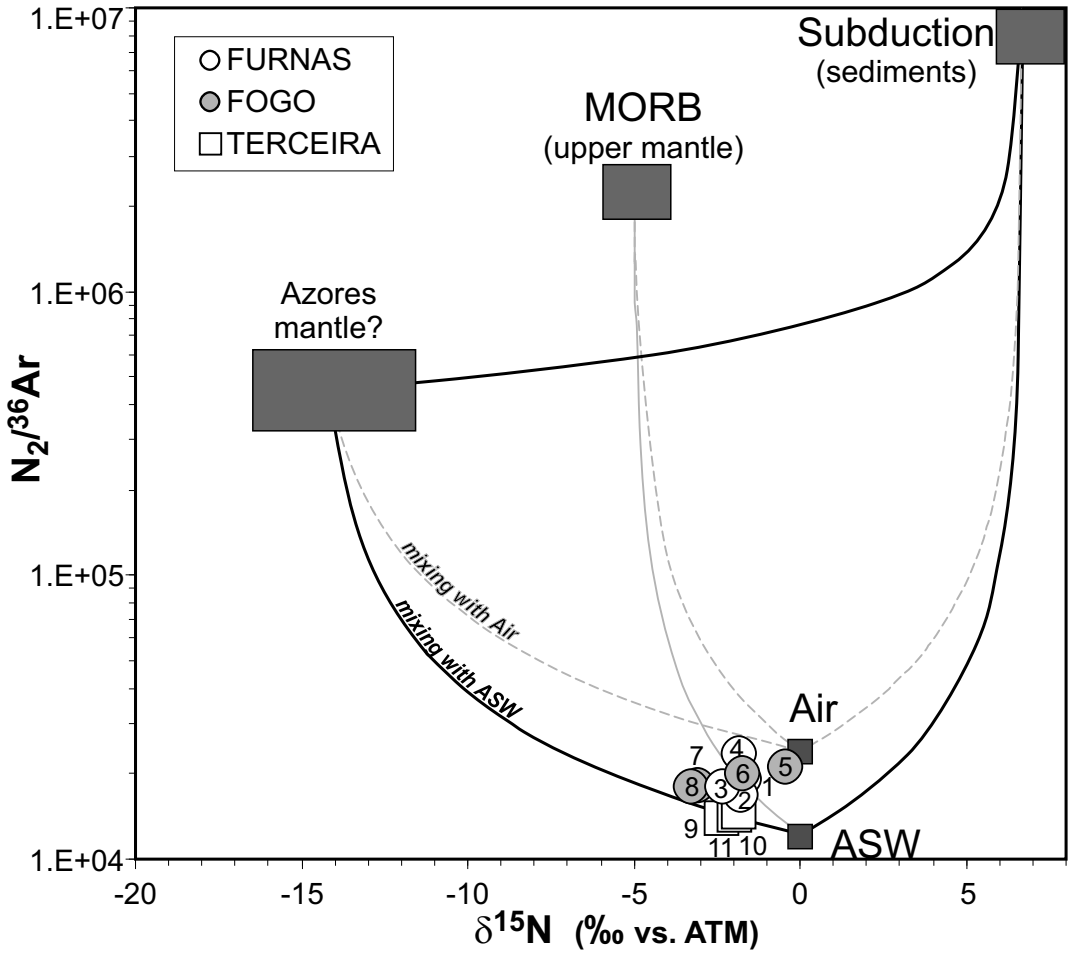
1.E+07
1.E+06
1.E+05
1.E+04
$N_2/^{36}Ar$
FURNAS
FOGO
TERCEIRA
Subduction
(sediments)
MORB
(upper mantle)
Azores
mantle?
mixing with Air
mixing with ASW
Air
ASW
7
4
6
5
8
3
2
1
9
11
10
-20
-15
-10
-5
0
5
$\delta^{15}N$ (‰ vs. ATM)

Figure 10

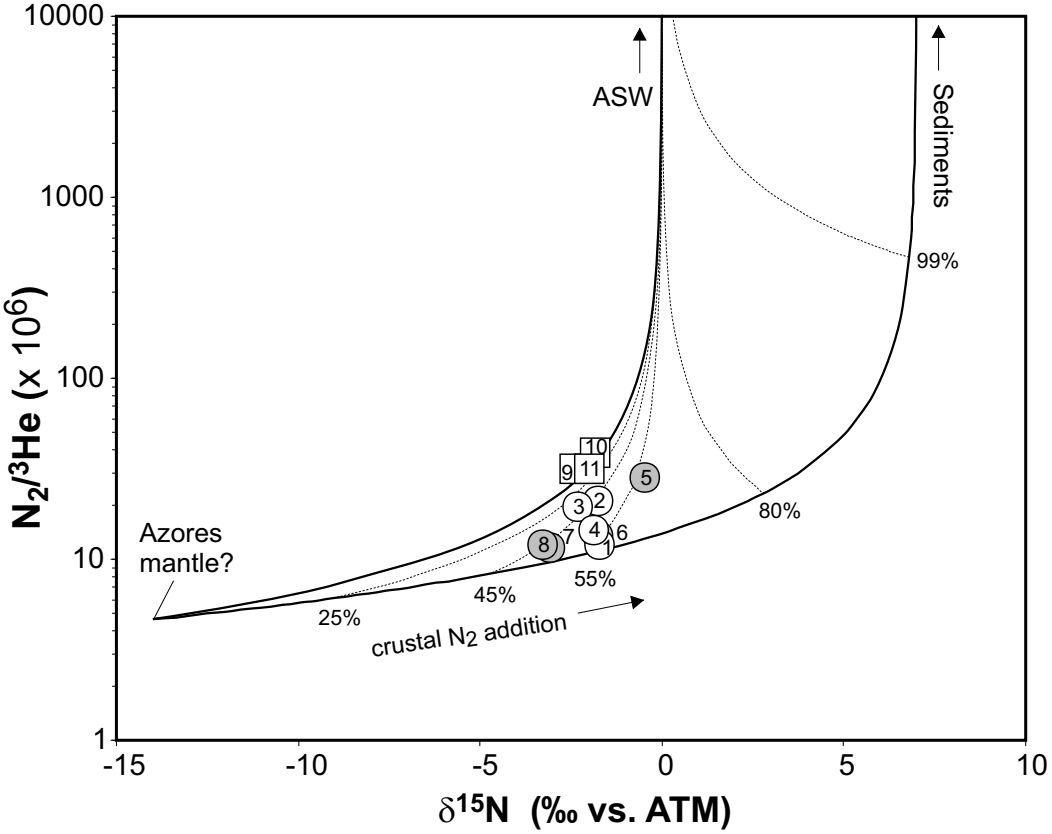
10000
1000
100
10
1
-15
-10
-5
0
5
10
N2/3He (x 10^6)
δ15N (‰ vs. ATM)
ASW
Sediments
99%
80%
55%
45%
25%
Azores
mantle?
crustal N2 addition
1
2
3
4
5
6
7
8
9
10
11

Figure 11

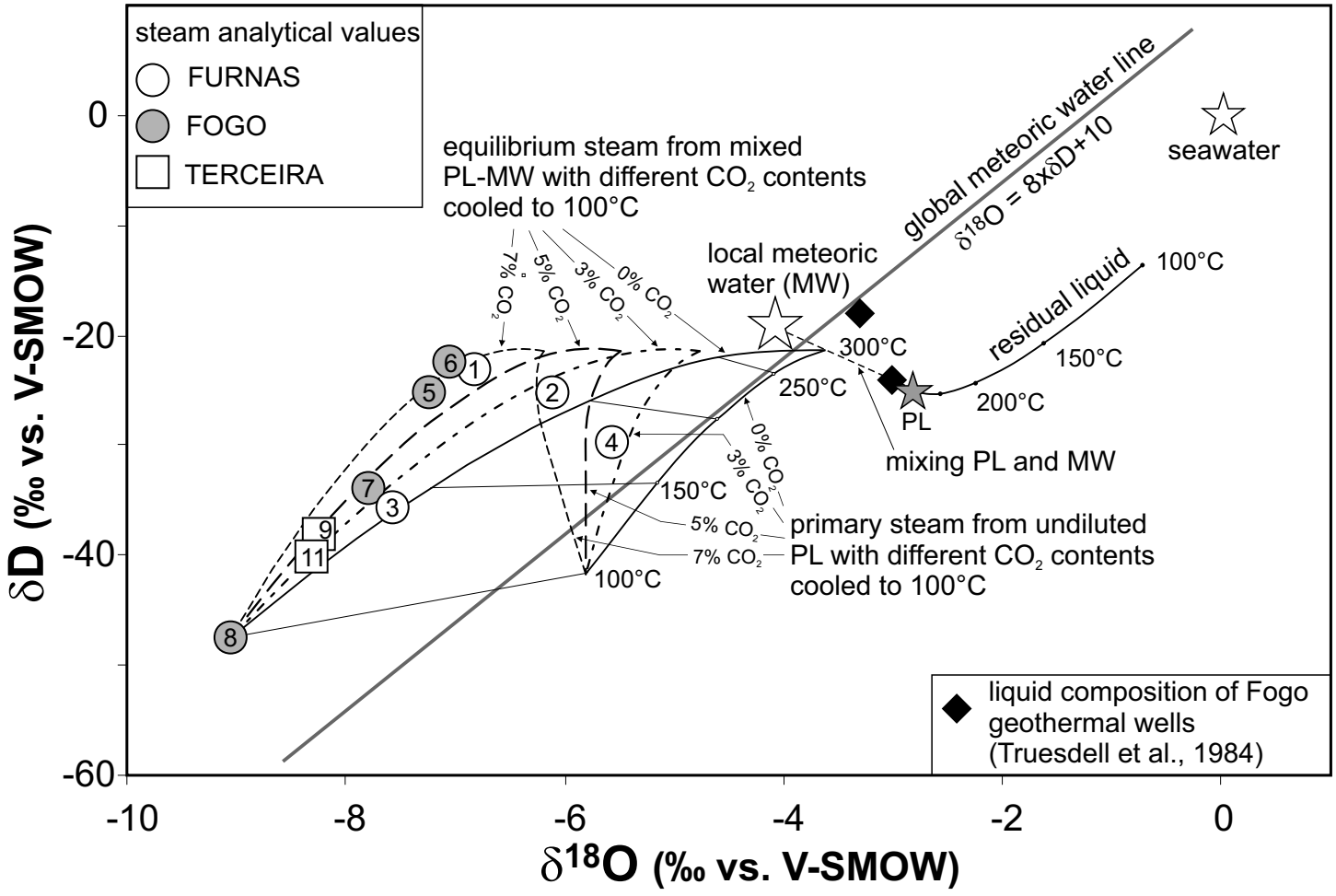
steam analytical values
FURNAS
FOGO
TERCEIRA
equilibrium steam from mixed PL-MW with different CO_2 contents cooled to 100°C
7% CO_2
5% CO_2
3% CO_2
0% CO_2
local meteoric water (MW)
global meteoric water line
$\delta^{18}O = 8x\delta D+10$
seawater
residual liquid
100°C
150°C
200°C
250°C
300°C
PL
mixing PL and MW
primary steam from undiluted PL with different CO_2 contents cooled to 100°C
liquid composition of Fogo geothermal wells (Truesdell et al., 1984)
δD (‰ vs. V-SMOW)
$\delta^{18}O$ (‰ vs. V-SMOW)
0
-20
-40
-60
-10
-8
-6
-4
-2
0

Figure 12

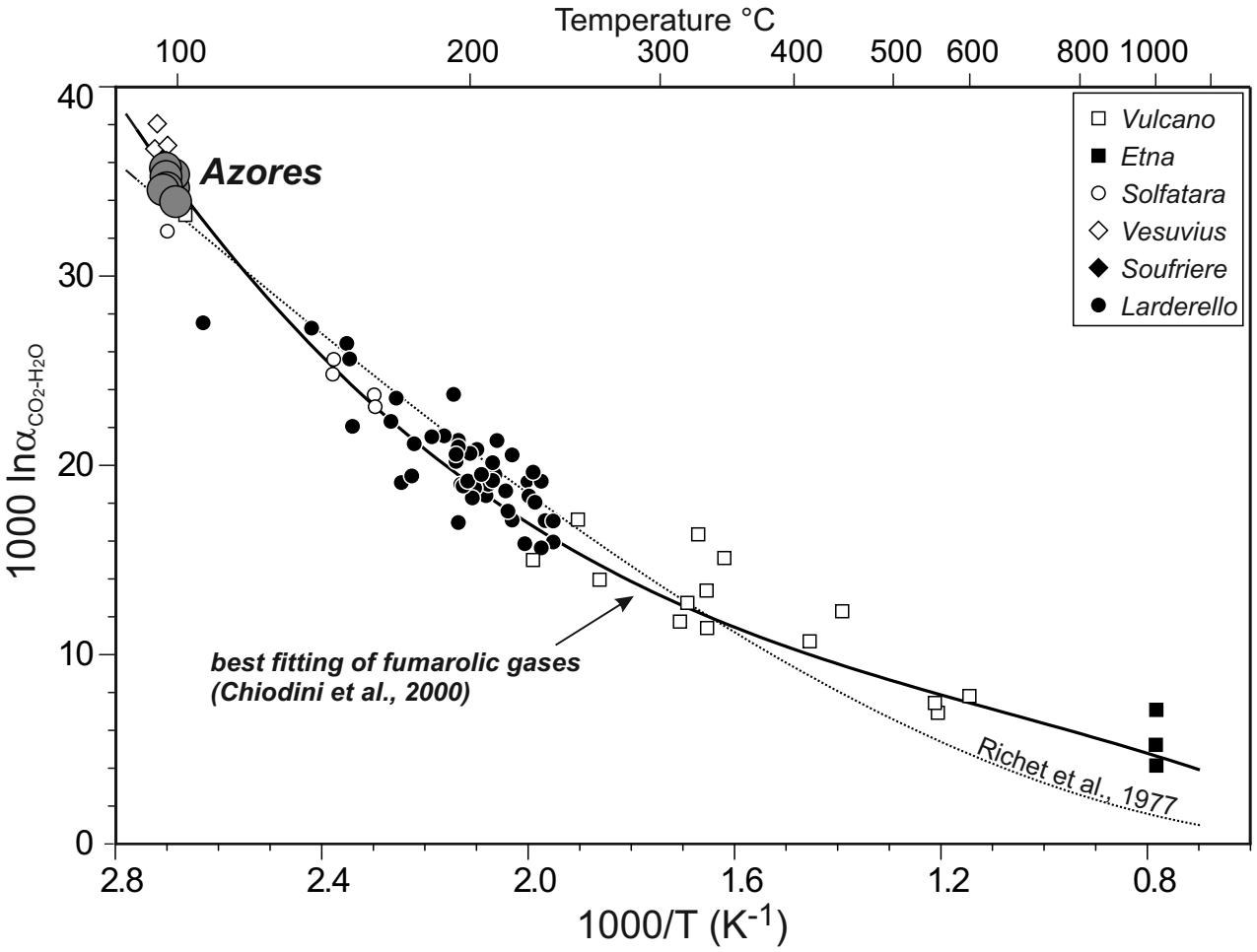
Temperature °C
100
200
300
400
500
600
800
1000
40
30
20
10
0
1000 lnα$_{CO_2-H_2O}$
Azores
Vulcano
Etna
Solfatara
Vesuvius
Soufriere
Larderello
best fitting of fumarolic gases
(Chiodini et al., 2000)
Richet et al., 1977
2.8
2.4
2.0
1.6
1.2
0.8
1000/T (K^{-1})

Figure 13

Nc	Sample	Locality	Date	UTM_E	UTM_N	T°C	H_2O	CO_2	H_2S	^{40}Ar	O_2	N_2	CH_4	H_2	He	CO	$^{40}Ar/^{36}Ar$	$\delta^{15}N$	$\delta^{18}O_{steam}$	δD_{steam}	$\delta^{13}C_{CO2}$	$\delta^{18}O_{CO2}$	R/Ra c	He/Ne	To(°C)	Ts(°C)
1	Furnas Lagoa	S.Miguel, Furnas	21/09/2013	646957	4181459	96.7	938000	61900	199	1.51	0.007	73	1.12	54.1	0.832	0.125	399	-1.72	-6.84	-22.9	-4.21	28.4	5.23 ± 0.054	54.4	276	271
2	Ribeira dos Tambores	S.Miguel, Furnas	21/09/2013	650240	4181700	98.0	932000	67400	150	3.40	n.d.	156	7.18	74.2	1.00	0.0297	371	-1.78	-6.11	-25.0	-3.85	28.7	5.37 ± 0.055	45.8	202	202
3	Ribeira Tambores River	S.Miguel, Furnas	23/09/2013	650374	4181520	99.7	960000	39200	176	1.70	n.d.	80.3	5.65	89.8	0.557	0.0237	386	-2.33	-7.59	-35.5	-3.73	26.8	5.34 ± 0.054	56.4	209	209
4	Caldeira Seca	S.Miguel, Furnas	21/09/2013	649342	4181952	98.9	956000	43700	244	1.10	n.d.	54.7	2.00	95.2	0.523	0.0439	479	-1.87	-5.56	-29.7	-3.77	29.6	5.27 ± 0.055	40.9	229	229
5	Caldeiras da Ribeira Grande	S.Miguel, Fogo	19/09/2013	633209	4184470	97.8	941000	58300	182	2.29	n.d.	145	2.25	129	0.708	0.148	345	-0.48	-7.24	-25.1	-3.98	28.1	5.26 ± 0.056	42.1	260	259
6	Caldeiras da Ribeira Grande	S.Miguel, Fogo	26/09/2013	633209	4184470	96.4	944000	55200	169	1.26	n.d.	63.8	2.02	113	0.642	0.0261	399	-1.75	-7.06	-22.4	-3.97	28.1	5.38 ± 0.054	42.3	189	188
7	RG4 Geoth. well A	S.Miguel, Fogo	19/09/2013	632933	4184331	99.3	947000	53100	38.6	1.26	0.007	58.2	2.19	114	0.684	0.195	393	-3.08	-7.8	-33.9	-3.89	28.0	5.27 ± 0.056	52.4	281	278
8	RG4 Geoth. well B	S.Miguel, Fogo	26/09/2013	632951	4184320	97.3	956000	43800	11.4	1.09	0.049	49.9	1.76	111	0.57	0.133	396	-3.29	-9.05	-47.5	-4.14	26.2	5.27 ± 0.056	64.0	274	272
9	Furnas Enxofre	Terceira, Pico Alto	04/10/2013	479846	4286810	96.9	968000	30900	255	3.02	n.d.	136	143	273	0.324	0.0377	311	-2.40	-8.26	-38.1	-4.48	27.8	9.60 ± 0.098	30.6	192	192
10	Furnas Enxofre	Terceira, Pico Alto	04/10/2013	479841	4286823	97.0	965000	34100	269	3.30	7.15	165	146	276	0.32	0.0416	299	-1.85	n.a.	n.a	-4.62	27.5	9.59 ± 0.10	27.9	191	191
11	Furnas Enxofre	Terceira, Pico Alto	04/10/2013	479840	4286815	97.0	962000	37200	322	3.89	n.d.	185	185	347	0.442	0.0456	304	-1.99	-8.32	-40.1	-4.66	27.4	9.59 ± 0.10	27.9	181	181